

The Significance of 2-Furyl Ring Substitution with a 2-(*para*-substituted) Aryl Group in a New Series of Pyrazolo-triazolo-pyrimidines as Potent and Highly Selective hA₃ Adenosine Receptors Antagonists: New Insights into Structure–Affinity Relationship and Receptor–Antagonist Recognition

Siew Lee Cheong,[†] Anna Dolzhenko,[†] Sonja Kachler,[‡] Silvia Paoletta,[§] Stephanie Federico,^{||} Barbara Cacciari,[⊥] Anton Dolzhenko,[†] Karl-Norbert Klotz,[‡] Stefano Moro,^{*,§} Giampiero Spalluto,^{*,||} and Giorgia Pastorin^{*,†}

[†]Department of Pharmacy, National University of Singapore, 3 Science Drive 2, Block S15, no. 05-PI-03, Singapore 117543, [‡]Institut für Pharmakologie, Universität of Würzburg, D-97078 Würzburg, Germany, [§]Molecular Modeling Section (MMS), Dipartimento di Scienze Farmaceutiche, Università di Padova, via Marzolo 5, I-35131 Padova, Italy, ^{||}Dipartimento di Scienze Farmaceutiche, Università degli Studi di Trieste, Piazzale Europa 1, I-34127 Trieste, Italy, and [⊥]Dipartimento di Scienze Farmaceutiche, Università degli Studi di Ferrara, via Fossato di Mortara 17-19, I-44100 Ferrara, Italy

Received January 14, 2010

Among the heterocyclic structures identified as potent human A₃ (hA₃) adenosine receptor's antagonists, we have demonstrated that the new pyrazolo-triazolo-pyrimidines, bearing an aryl group in replacement of the C²-furyl ring, not only confer a good pharmacological profile (with significantly enhanced selectivity against other adenosine receptor subtypes) but also overcome the metabolic transformation of the furan ring into toxic intermediates. All the synthesized [2-(*para*-substituted) phenyl]-pyrazolo-triazolo-pyrimidines showed affinity at the hA₃ receptor in the low nanomolar range. The most potent derivative of the series presented better affinity and excellent selectivity (compound **31**, K_i hA₃ = 0.108 nM; hA₁/hA₃ = 5200; hA_{2A}/hA₃ = 7200), in comparison to the C²-furyl counterpart. A receptor-driven molecular modeling investigation, based on a recently proposed model of A₃ receptor derived from the crystallographic structure of human A_{2A} receptor, has been carried out in order to support the experimental binding data and to justify the enhanced selectivity against the other receptor subtypes.

Introduction

Human A₃ adenosine receptor (hA₃AR), a member of the seven transmembrane domains G-protein-coupled receptor (GPCR⁴) family, modulates several physiopathological conditions.^{1,2} Its inhibition through selective hA₃ antagonists is found to be beneficial in inflammatory, asthmatic and ischemic conditions.³ In addition, the A₃ receptors have been shown to be overexpressed in some tumor cell lines, suggesting that this receptor could be a potential target in cancer therapy.⁴ However, different from the other adenosine receptor subtypes (A₁, A_{2A}, and A_{2B}, respectively), there are remarkable species differences in the case of A₃ receptor,^{5,6}

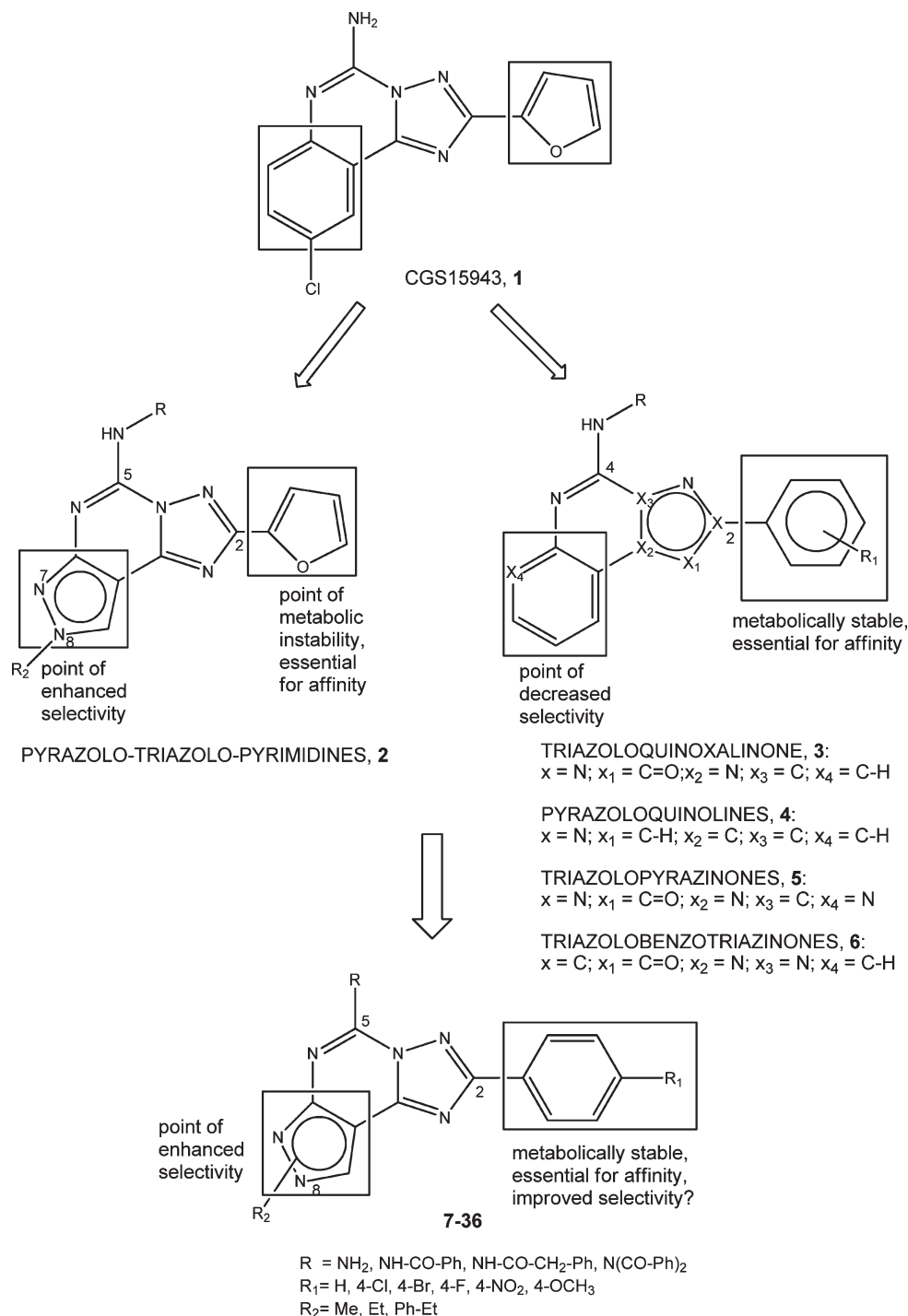
which render the discovery of new selective compounds more unpredictable and complicated.

Among the several diverse structures that have demonstrated affinity at the hA₃ adenosine receptor, our group has particularly focused on the development of compounds bearing a pyrazolo-triazolo-pyrimidine (PTP) nucleus (**2**) (Chart 1).^{7,8} The PTP tricyclic nucleus resembles the triazolo-quinoline core of nonselective antagonist CGS15943 (**1**),⁹ except for the phenyl ring being replaced by a pyrazole, which has resulted in an increase of selectivity against other receptor subtypes.¹⁰ Further exploitation of substituents, mainly at positions N⁸ and N⁵ of such structure,^{10,11} has given rise to highly potent and moderately selective hA₃ antagonists. In particular, the combination of a methyl group at N⁸ and a 4-pyridyl carbamoyl chain at N⁵ has led to the most potent hA₃ antagonist ever synthesized.¹² Conversely, substitution at position C² of the PTP tricyclic system has not been deeply explored, being essentially limited to the introduction of a furyl group. The furan ring has been considered as an essential structural requirement for the binding of antagonists at all the adenosine receptor subtypes, while its removal from the tricyclic system has been associated with an irreversible loss of affinity and selectivity, regardless of the receptor under investigation.

To reiterate, Baraldi and co-workers¹³ have found that the substitution of the furan ring in PTPs with phenyl or alkoxy-phenyl rings led to a loss of affinity at A_{2A}, A_{2B}, and A₃ receptors, while the A₁ subtype in some cases displayed a high

*To whom correspondence should be addressed. For G. P.: phone, +65 6516 1876; fax, +65 6779 1554; E-mail, phapg@nus.edu.sg. For S. M.: phone, +39-049-8275704; E-mail, stefano.moro@unipd.it. For G. S.: phone, +39-040-558-3726; E-mail, spalluto@univ.trieste.it.

[†]Abbreviations: APCI, atmospheric pressure chemical ionization; AR, adenosine receptor; ATP, adenosine triphosphate; cAMP, cyclic adenosine monophosphate; CHO cells, Chinese hamster ovary cells; DIPEA, diisopropylethylamine; EGTA, ethylene glycol tetraacetic acid; EL2, extracellular loop 2; EtOAc, ethyl acetate; GPCR, G-protein-coupled receptor; [³H]-CCPA, [³H]-2-chloro-6-cyclopentyl adenosine; [³H]-NECA, [³H]-*N*-ethylcarboxamido adenosine; HPLC, high performance liquid chromatography; MgCl₂, magnesium chloride; MOE, Molecular Operating Environment software; NaCl, sodium chloride; NaH, sodium hydride; Na₂SO₄, sodium sulfate; PTP, pyrazolo-triazolo-pyrimidine; rmsd, root-mean-square deviation; R-PIA, R-*N*⁶-phenylisopropyladenosine; SAR, structure–affinity relationship; TEA, triethylamine; TLC, thin-layer chromatography; TM, transmembrane.

Chart 1. Rationale for the Design of 2-(*para*-substituted)phenyl Pyrazolo-triazolo-pyrimidine Derivatives

nanomolar binding profile. Similarly, the functionalization of the furan ring with polar substituents resulted in completely inactive derivatives, clearly indicating that an unsubstituted furan ring at the C² position played a fundamental role in ligand–receptor recognition. Notably, in most cases, substitution at the pyrazole ring occurred at the N⁷ rather than at the N⁸ position; hence, these compounds might not reflect the same binding profile as their N⁸ analogues. This observation has triggered our interest to further investigate the effect of concurrent substitution of alkyl groups at N⁸ position and a different moiety (other than furan ring) at the C² position of PTPs on the affinity at hA₃ receptor and selectivity over other

adenosine receptor subtypes. Interestingly, several reported hA₃ antagonists bearing tricyclic scaffolds (which are also structural resemblance of CGS15943 (**1**), including triazoloquinoxalines (**3**),^{14,15} pyrazoloquinolines (**4**),¹⁶ triazolopyrazinones (**5**),¹⁷ and triazolobenzotriazinones (**6**)¹⁸ (Chart 1)), comprise a substituted phenyl moiety at the position equivalent to that of furan ring in PTP derivatives. From the structure–affinity relationship (SAR) studies of these derivatives, the presence of the phenyl ring seemed crucial to maintain good affinity at hA₃ receptor. In light of the beneficial effect of this phenyl ring toward the hA₃ affinity, the substitution of the C²-furyl ring with an aryl group is

therefore deemed feasible for the design and synthesis of new series of PTPs.

From the pharmacokinetic aspect, several studies reported that drugs containing a furan in their chemical structure (e.g., prazosin and frusemide) were subjected to a metabolic cleavage of the furyl ring by the cytochrome P450 enzymes in the liver,^{19–21} resulting in remarkable hepatotoxicity in treated mice.²⁰ Some of these intermediate metabolites, for example epoxide groups and γ -keto- α,β -unsaturated aldehydes, were shown to be reactive and able to form adducts with cellular proteins or DNA, therefore causing unpredictable effects. Although these reactive metabolites can be detoxified by several enzymes in the body, this still poses some threat of toxicity and should be regarded as a safety issue. On the other hand, metabolites derived from biotransformation of the phenyl ring through oxidation by CYP450 enzymes are expected to be relatively less reactive than those found in the metabolism of furan ring. Furthermore, the typical oxidation targeted at the *para*-position of the phenyl ring can be bypassed through the synthesis of *para*-substituted derivatives, leading to improvement of bioavailability of the new bioactive compounds.

On the basis of potential structural and metabolic benefits of the C²-aryl group in PTP derivatives, a novel structure–affinity relationship evaluation was conducted through the rational design and synthesis of a new series of pyrazolo-triazolo-pyrimidines bearing a (*para*-substituted)-phenyl ring at C², while maintaining either methyl or phenyl-ethyl groups at N⁸ and a free amino, phenylacetamide or (bis-)benzamide at the N⁵ position (compounds 7–36).

Moreover, in order to rationalize the observed structure–affinity relationship and the selectivity profile of this new series of derivatives, a receptor-driven molecular modeling investigation, based on a recently proposed model of hA₃ receptor derived from the crystallographic structure of human A_{2A} receptor,²² was also performed in this study.

Chemistry

The synthetic pathways of new series of 2-(*para*-substituted)phenyl-pyrazolo-[4,3-*e*]1,2,4-triazolo[1,5-*c*]pyrimidines derivatives 7–36 (Chart 1) are depicted in Schemes 1 and 2. Compounds 7–20 were prepared following similar procedures as already described elsewhere for the synthesis of the pyrazolo-[4,3-*e*]1,2,4-triazolo[1,5-*c*]pyrimidines^{10,23} (Scheme 1). The inseparable mixture of 1-alkyl-5-amino-4-cyano-pyrazole and 2-alkyl-5-amino-4-cyano-pyrazole regioisomers (39–42) for both the ethyl and phenylethyl series were synthesized as described in ref 10. For compounds bearing a methyl group, an alternative procedure was followed to obtain only the 2-methyl-5-amino-4-cyano-pyrazole isomer (38) in good yield.²³ The obtained intermediates were directly refluxed in triethyl orthoformate to give the corresponding imidates (43–47), which were subsequently reacted with the appropriate (*para*-substituted)benzoic hydrazide in refluxing 2-methoxy-ethanol to afford the intermediates 48–61. Subsequently, these compounds were subjected to a thermally induced cyclization in diphenyl ether at 260 °C. After the chromatographic separation of N⁷ (minor product) and N⁸ (major product) regioisomers, they provided the tricyclic compounds (62–75) in rather good yield (about 60% for N⁸ derivatives and 30% for N⁷ derivatives). Hydrolysis in 20% HCl gave rise to the corresponding hydrolyzed intermediates (76–89), which were subsequently converted into the 5-amino-7 or 8-(substituted)-2-[(*para*-substituted)phenyl]pyrazolo-[4,3-*e*]1,2,4-triazolo[1,5-*c*] pyrimidine derivatives (7–20).

Some of the compounds bearing either a methyl group (7–12) or a phenylethyl group (15, 19) at N⁸ were dispersed in toluene and treated with either benzoic anhydride or phenylacetyl chloride (Scheme 2). The mixture was heated under reflux and stirred for 6–12 h. The solvent was removed under reduced pressure, and the residue was crystallized from an appropriate solvent or subjected to chromatographic purification, to afford the desired compounds (21–26, 29–36). On top of that, two additional compounds, obtained from the reaction of compounds 9 and 11 with benzoyl chloride, were further isolated from the alcoholic mixtures of methanol or ethanol: they included the bis-acylated products 27 and 28.

Biological Assay

1. Binding Affinity at Human A₁, A_{2A}, and A₃ Adenosine Receptors. The affinity of an antagonist toward its receptor (expressed in Chinese hamster ovary cells (CHO) for hA₁, hA_{2A}, hA₃ receptors) was evaluated through the measurement of displacement of selective radioligands,^{24–27} which were previously bound to the receptor expressed at the cell surface. In this assay, we evaluated the displacement of: (i) specific [³H]CCPA binding at hA₁ receptors, (ii) specific [³H]NECA binding at both the hA_{2A} and hA₃ receptors. The data were expressed as K_i (dissociation constant), which was calculated from the Cheng and Prusoff equation,²⁷ with geometric means of at least three experiments, including 95% confidence intervals.

2. Adenylyl Cyclase Activity. Because of the lack of a suitable radioligand for hA_{2B} receptor in binding assay, the potency of antagonists at hA_{2B} receptor (expressed on CHO cells) was determined in adenylyl cyclase experiments instead. The procedure was carried out as described previously in Klotz et al. with minor modifications.^{24,25} In this assay, an adenosine agonist (NECA) at known concentration was subjected to inhibitory effect of tested antagonist. As a result, the activation of adenylyl cyclase was inhibited with decrease in the cAMP (cyclic adenosine monophosphate) production.

Molecular Modeling

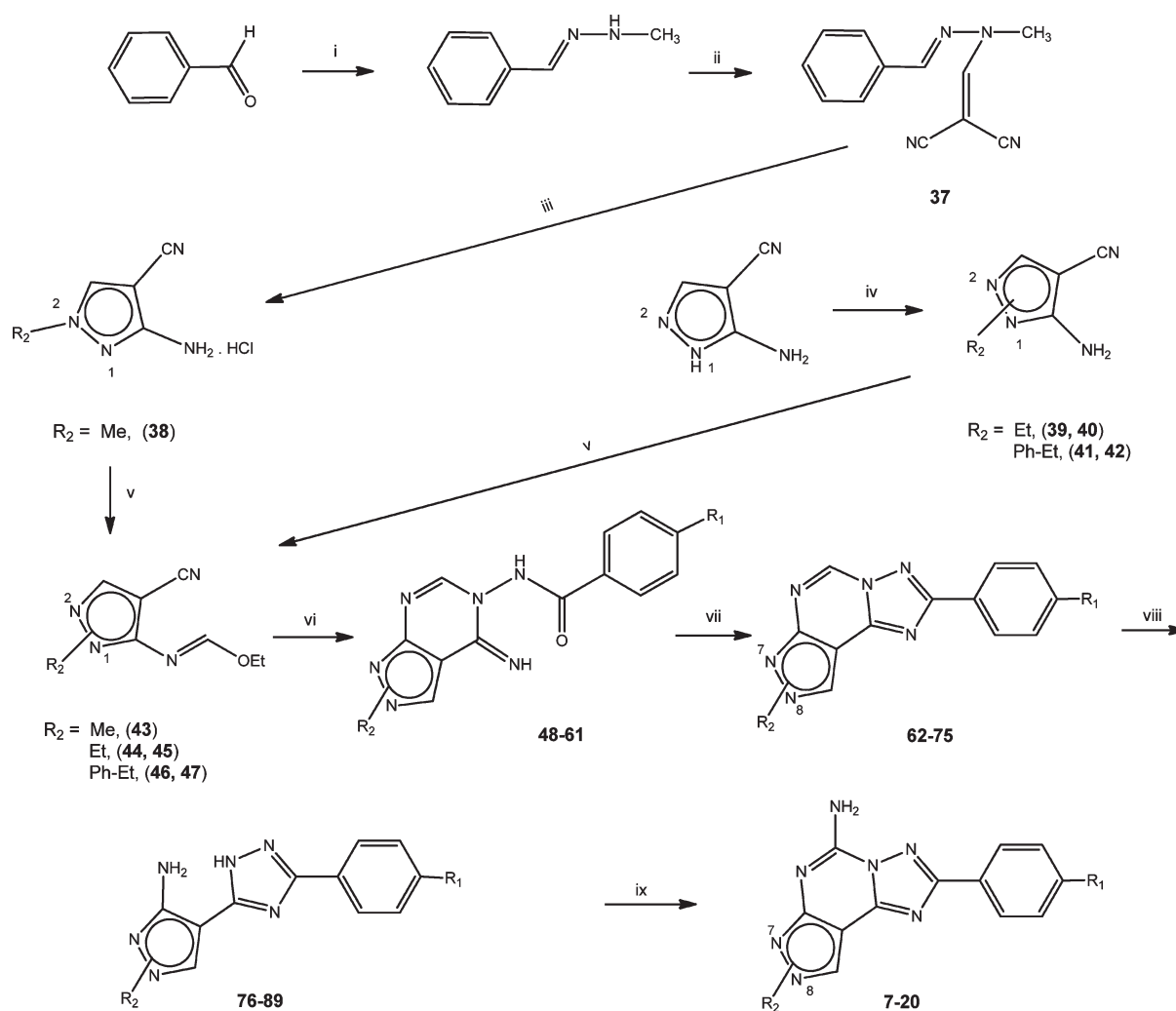
The recently published crystallographic structure of human A_{2A} adenosine receptor, in complex with the high affinity antagonist ZM241385 (PDB code: 3EML),²² provided a new alternative template to perform homology modeling of other GPCRs, particularly the adenosine receptors. Therefore, we built up a homology model of the hA₃ receptor based on the crystal structure of the hA_{2A} receptor.^{28,29}

In the process of selecting a reliable docking protocol to be employed in the following docking studies of these new derivatives, we have evaluated the ability of different docking softwares to reproduce the crystallographic pose of ZM241385 inside the binding cavity of hA_{2A} receptor. As reported in the Experimental Section, among the four different types of programs used to calibrate our docking protocol, the GOLD program was finally chosen because it showed the best performance with regards to the calculated rmsd values relative to the crystallographic pose of ZM241385.²⁸

Consequently, based on the selected docking protocol, we performed the docking simulations to identify the hypothetical binding mode of the new series of 2-(*para*-substituted)-phenyl-PTPs inside the hA₃ and hA_{2A} adenosine receptors.

Results and Discussion

A. Structure–Affinity Relationship Studies. A new series of 2-(*para*-substituted)phenyl-pyrazolo[4,3-*e*]1,2,4-triazolo-[1,5-*c*]pyrimidines was successfully synthesized and characterized.

Scheme 1. Synthetic Scheme for Compounds 7–20^a

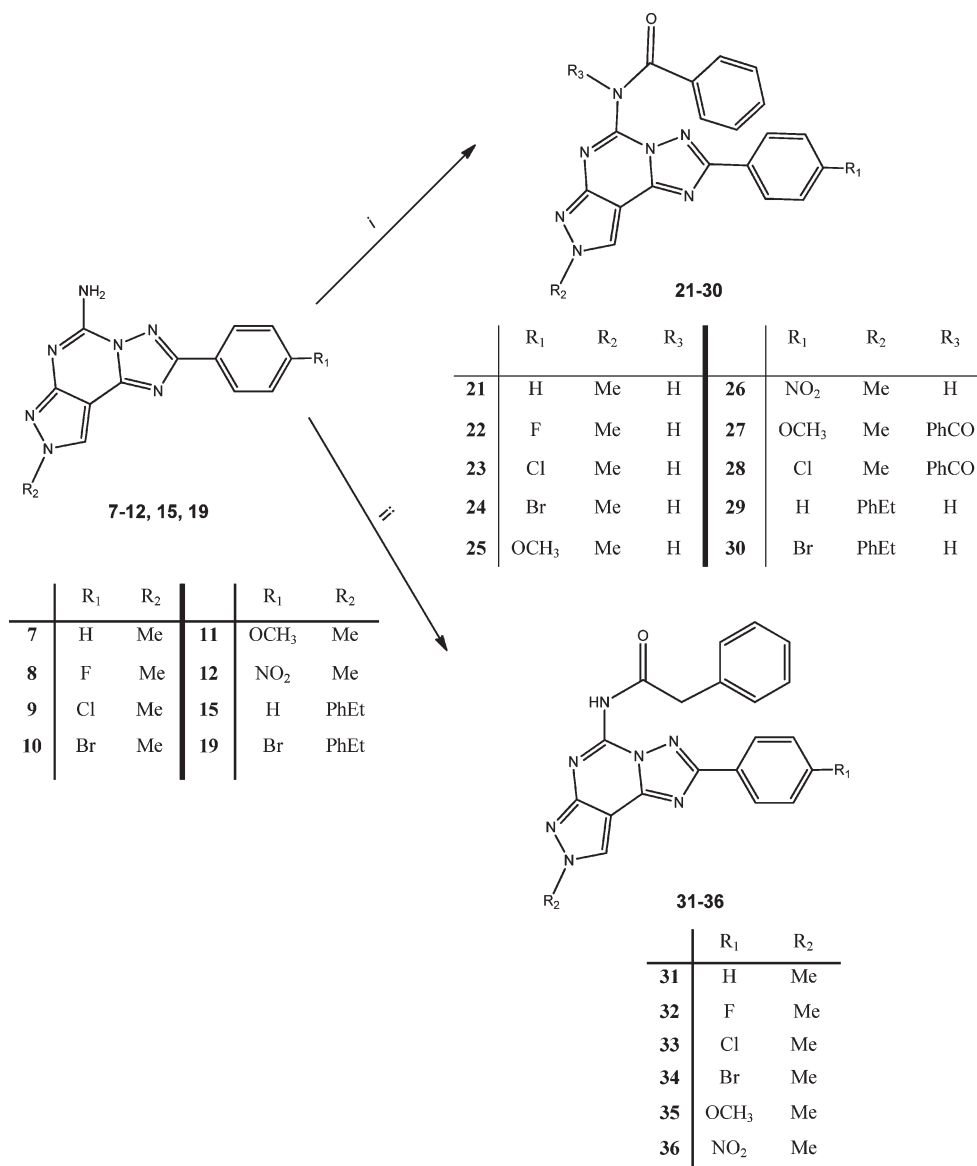
	R ₁	R ₂		R ₁	R ₂
7	H	N ⁸ -Me	14	Cl	N ⁸ -Et
8	F	N ⁸ -Me	15	H	N ⁸ -PhEt
9	Cl	N ⁸ -Me	16	F	N ⁸ -PhEt
10	Br	N ⁸ -Me	17	Cl	N ⁷ -PhEt
11	OCH ₃	N ⁸ -Me	18	Cl	N ⁸ -PhEt
12	NO ₂	N ⁸ -Me	19	Br	N ⁸ -PhEt
13	Cl	N ⁷ -Et	20	OCH ₃	N ⁸ -PhEt

^a Reagents: (i) 2-methylhydrazine, absolute EtOH; (ii) ethoxymethylene-malononitrile, benzene; (iii) conc HCl; (iv) NaH, R₂X, dimethylformamide; (v) HC(OEt)₃, reflux; (vi) 2-(4-substituted)benzoic hydrazide, MeO(CH₂)₂OH; (vii) Ph₂O, 260 °C, flash chromatography; (viii) HCl, reflux; (ix) NH₂CN, 1-methyl-2-pyrrolidinone, pTsOH.

Table 1 summarizes the receptor binding affinities of compounds 7–36 determined at the human A₁, A_{2A}, and A₃ receptors and the corresponding adenylyl cyclase activity in CHO cells which express the A_{2B} receptors.

We introduced very little modifications in the pyrazole ring in order to focus our investigation on the exploitation at position C². In fact, only two compounds (compounds 13 and 17, bearing a substituent at N⁷ instead of N⁸) were strategically included in the library to confirm the necessity to have

a small alkyl group at N⁸ for an optimal interaction with the hA₃ receptor subtype.¹⁰ For the rest of the derivatives, we fixed the methyl (compounds 7–12), ethyl (compound 14), and phenylethyl (compounds 15, 16, 18–20) groups at N⁸, with concurrent introduction of different moieties at positions C² and N⁵ (compounds 21–36). The binding assay results showed that the new series of 2-aryl-pyrazolo-triazolo-pyrimidines presented good affinity at hA₃ receptors, as indicated by low nanomolar range of K_i values and

Scheme 2. Synthetic Scheme for Compounds **21–36**^a

^a Reagents: (i) benzoic anhydride, toluene (in synthesis of **21–26**, **29**, **30**) or benzoyl chloride with DIPEA/TEA in toluene/dioxan (in synthesis of **27**, **28**), reflux; (ii) phenylacetyl chloride, DIPEA, toluene, reflux.

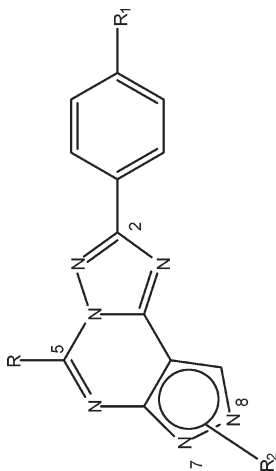
considerably improved selectivity toward the other AR subtypes (Table 1).

C² Position. To examine the impact of the furan ring substitution with a phenyl ring at C² position toward the pharmacological profile, we compared the binding assay results of compounds bearing the 2-furyl (e.g., compounds **90** and **91**) (Table 2)^{10,30} and the 2-aryl (e.g., compounds **7** and **31**). It was observed that the bioisosteric replacement of existing furan ring with a phenyl ring resulted in a 3–7-fold increase in affinity toward the hA₃ receptor and significant improvement in selectivity (of 2–3 order of magnitude) over other adenosine receptor subtypes, namely hA₁, hA_{2A}, and hA_{2B} receptors. In other words, compounds with a phenyl ring at 2-position have demonstrated better affinity and selectivity profiles toward hA₃ receptor as compared to the 2-furyl counterparts, indicating that the aryl group at C² position played a more essential role on the antagonistic activity at the hA₃ receptor.

The substituents (e.g., Cl, F, Br, OCH₃, NO₂) at the *para* position of the C²-phenyl ring were found to modulate the

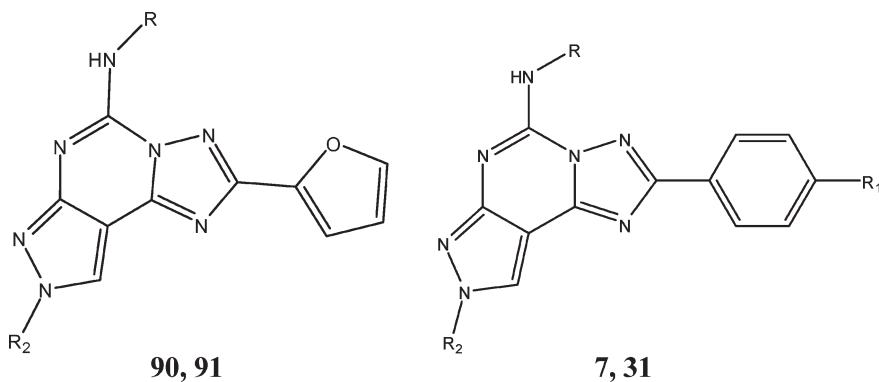
affinity at hA₃AR to a certain extent. In particular, among the substituents introduced at the *para* position of phenyl ring, both the OCH₃ and F groups have exerted relatively more favorable effect on the affinity at hA₃ receptor in all the N⁵-unsubstituted (e.g., compound **11**, with K_ihA₃ = 16.7 nM, hA₁/hA₃ = 583; hA_{2A}/hA₃ = 71.3), N⁵-benzamide-substituted (e.g., compound **25**, with K_ihA₃ = 2.1 nM, hA₁/hA₃ = > 14300; hA_{2A}/hA₃ = > 47600) and N⁵-phenylacetamide-substituted (e.g., compound **35**, with K_ihA₃ = 0.241 nM; hA₁/hA₃ > 124,000; hA_{2A}/hA₃ > 415000) derivatives.

Interestingly, although all the compounds with a 4-bromo group in the N⁸-methyl series showed good affinity at the hA₃ receptor (e.g., compound **34**, with K_ihA₃ = 0.345 nM; hA₁/hA₃ = 70700; hA_{2A}/hA₃ > 290000), its presence in the N⁸-phenylethyl-substituted derivatives (e.g., compound **30**, with K_ihA₃ = 153 nM; hA₁/hA₃ = 1.76; hA_{2A}/hA₃ > 654) caused the opposite effect to the affinity at hA₃ receptor. This could be possibly due to the additional steric hindrance caused by the phenylethyl group, which further limited the

Table 1. Binding Affinity (K_i) at hA_1 , hA_{2A} , hA_{2B} , and hA_3 Receptors and Selectivity against hA_1 and hA_{2A} Receptors


compd	R	R_1	R_2	K_i , nM (95% CI)				selectivity	
				hA_1^a	hA_{2A}^b	hA_{2B}^c	hA_3^d	hA_1/hA_3	hA_{2A}/hA_3
7	NH ₂	H	N ⁸ -CH ₃	339 (319–359)	121 (100–147)	> 10000	75 (63.1–90.4)	4.52	1.61
8	NH ₂	F	N ⁸ -CH ₃	1010 (815–1240)	355 (307–409)	> 10000	31.4 (26.9–36.6)	32.2	11.3
9	NH ₂	Cl	N ⁸ -CH ₃	4860 (3360–7010)	2020 (1060–3840)	> 10000	72.4 (71.3–73.6)	67.1	27.9
10	NH ₂	Br	N ⁸ -CH ₃	2890 (2230–3730)	1500 (1370–1640)	> 10000	38.6 (35.9–41.5)	74.9	38.9
11	NH ₂	OCH ₃	N ⁸ -CH ₃	9730 (7740–12200)	1190 (1050–1340)	> 10000	16.7 (9.80–28.3)	583	71.3
12	NH ₂	NO ₂	N ⁸ -CH ₃	> 300000	9650 (5490–16900)	> 10000	655 (563–763)	> 458	14.7
13	NH ₂	Cl	N ⁷ -CH ₂ -CH ₃	121 (94.9–154)	83.8 (42.3–166)	> 10000	565 (518–615)	0.21	0.15
14	NH ₂	Cl	N ⁸ -CH ₂ -CH ₃	1570 (1350–1820)	843 (566–1260)	> 10000	68.7 (52.9–89.3)	22.9	12.3
15	NH ₂	H	N ⁸ -CH ₂ -CH ₂ -Ph	74.8 (51.9–108)	196 (121–317)	> 10000	76.7 (59.5–99.0)	0.975	2.56
16	NH ₂	F	N ⁸ -CH ₂ -CH ₂ -Ph	39.1 (31.9–47.9)	127 (106–151)	> 10000	50.6 (32.9–78.0)	0.773	2.51
17	NH ₂	Cl	N ⁷ -CH ₂ -CH ₂ -Ph	> 100000	5970 (4090–8720)	> 10000	> 30000	> 3	< 0.2
18	NH ₂	Cl	N ⁸ -CH ₂ -CH ₂ -Ph	204 (159–262)	2180 (1400–3410)	> 10000	79.7 (67.9–93.6)	2.56	27.4
19	NH ₂	Br	N ⁸ -CH ₂ -CH ₂ -Ph	498 (327–758)	> 30000	> 10000	221 (152–320)	2.25	> 136
20	NH ₂	OCH ₃	N ⁸ -CH ₂ -CH ₂ -Ph	289 (232–359)	1400 (895–2210)	> 10000	25 (17.5–35.6)	11.6	56
21	NH-COPh	H	N ⁸ -CH ₃	622 (498–779)	324 (265–396)	> 10000	5 (2.93–5.56)	124	64.8
22	NH-COPh	F	N ⁸ -CH ₃	2530 (1550–4120)	> 100000	> 10000	3.43 (1.97–5.98)	738	> 29200
23	NH-COPh	Cl	N ⁸ -CH ₃	> 30000	> 100000	> 10000	2.82 (2.24–3.56)	> 10600	> 35500
24	NH-COPh	Br	N ⁸ -CH ₃	> 30000	> 100000	> 10000	5.24 (4.16–6.60)	> 5730	> 19100
25	NH-COPh	OCH ₃	N ⁸ -CH ₃	> 30000	> 100000	> 10000	2.1 (1.37–3.24)	> 14300	> 47600
26	NH-COPh	NO ₂	N ⁸ -CH ₃	> 30000	> 100000	> 10000	56.4 (43.5–73.0)	> 532	> 1770
27	N(CO-Ph) ₂	OCH ₃	N ⁸ -CH ₃	> 10000	> 10000	> 10000	6.88 (3.94–12.0)	> 1450	> 1450
28	N(CO-Ph) ₂	Cl	N ⁸ -CH ₃	> 10000	> 10000	> 10000	6.94 (4.58–10.5)	> 1440	> 1440
29	NH-COPh	H	N ⁸ -CH ₂ -CH ₂ -Ph	313 (209–468)	963 (749–1240)	> 10000	23.9 (20.3–28.1)	13.1	40.3
30	NH-COPh	Br	N ⁸ -CH ₂ -CH ₂ -Ph	270 (191–382)	> 100000	> 10000	153 (120–195)	1.76	> 654
31	NH-COCH ₂ Ph	H	N ⁸ -CH ₃	562 (446–706)	778 (554–1090)	> 10000	0.108 (0.089–0.131)	5204	7204
32	NH-COCH ₂ Ph	F	N ⁸ -CH ₃	2290 (1780–2930)	2540 (1590–4060)	> 10000	0.201 (0.175–0.230)	11400	12600
33	NH-COCH ₂ Ph	Cl	N ⁸ -CH ₃	4850 (3680–6400)	8320 (6180–11200)	> 10000	0.248 (0.211–0.292)	19600	33500
34	NH-COCH ₂ Ph	Br	N ⁸ -CH ₃	24400 (13900–42900)	> 100000	> 10000	0.345 (0.313–0.381)	70700	> 290000
35	NH-COCH ₂ Ph	OCH ₃	N ⁸ -CH ₃	> 30000	> 100000	> 10000	0.241 (0.214–0.272)	> 124000	> 415000
36	NH-COCH ₂ Ph	NO ₂	N ⁸ -CH ₃	23200 (9620–55700)	23900 (15300–37500)	> 10000	0.624 (0.529–0.735)	37179	38301

^a Displacement of specific [³H]-CCPA binding at human A_1 receptors expressed in CHO cells, ($n = 3-6$). ^b Displacement of specific [³H]-NECA binding at human A_{2A} receptors expressed in CHO cells, ($n = 3-6$). ^c K_i values of the inhibition of NECA-stimulated adenylyl cyclase activity in CHO cells, ($n = 3-6$). ^d Displacement of specific [³H]-NECA binding at human A_3 receptors expressed in CHO cells, ($n = 3-6$). Data are expressed as geometric means, with 95% confidence limits.

Table 2. Binding Affinity (K_i) at hA_3 Receptor and Selectivity against hA_1 and hA_{2A} Receptors for Compounds **90**, **91** and **7**, **31**

compd	R	R ₁	R ₂	hA_3 (K_i , nM)	hA_1/hA_3	hA_{2A}/hA_3
90	H		CH ₃	300 ^a	0.33 ^a	0.009 ^a
7	H	H	CH ₃	75	4.52	1.61
91	Ph-CH ₂ CO		CH ₃	0.81 ^a	867 ^a	522 ^a
31	Ph-CH ₂ CO	H	CH ₃	0.108	5204	7204

^aData taken from refs 10 and 30.

accommodation of relatively bulky bromo group within the binding site, resulting in detrimental effect on the hA_3 affinity. Besides that, it was observed that some N⁸-methyl-substituted compounds bearing a 2-(*para*-nitro)phenyl ring (e.g., compound **12**, $K_i hA_3 = 655$ nM; $hA_1/hA_3 > 458$; $hA_{2A}/hA_3 > 15.3$) have acquired hA_3 affinity in relatively high nanomolar range. Similarly, compound **26** (with a 2-(*para*-nitro) phenyl ring, a methyl at N⁸ and a benzamide at N⁵) only demonstrated moderate affinity at hA_3 receptor ($K_i hA_3 = 56.4$ nM) in comparison to the other derivatives with different substituents at C² position (compounds **22–25**), which have shown a better hA_3 affinity profile (2–5 nM). These observations could again be attributed to the steric constraint of the relatively bigger NO₂ group as compared to other substituents. This rendered the nitro group unable to bind firmly onto the binding cavity, thus affecting the affinity at the hA_3 receptor. Therefore, because the nitro group might not be a suitable substituent at this position, it was excluded from the subsequent series of N⁸-phenylethyl derivatives.

N⁵ Position. From the binding assay results, it was observed that the absence of any substituent at N⁵ position (such as in compounds **7–20**) did not allow good discrimination among the adenosine receptor subtypes, except for the hA_{2B} receptor. In other words, the free amino group at N⁵ not only bound to the hA_3 receptor but it also showed good interaction at both hA_1 and hA_{2A} receptors. This observation was consistent with previous SAR studies, which indicated high affinity at both hA_1 and hA_{2A} receptors in N⁵-unsubstituted derivatives.¹⁰ In fact, further incorporation of substituents at the N⁵ position (as shown in compounds **21–36**) enabled a shift of affinity toward the hA_3 subtype with a concomitant decrease of affinity at hA_1 and hA_{2A} receptors, thus improving selectivity in favor of the hA_3 subtype. This finding seemed to imply that the hA_3 binding cavity around the N⁵ position was rather spacious to accommodate the extended chains, in this case the benzoyl and phenyl acetyl groups. Between these two substituents, the longer phenyl acetyl group (e.g., compound **34**, with $K_i hA_3 = 0.345$ nM, $hA_1/hA_3 = 70700$; $hA_{2A}/hA_3 > 290000$) showed relatively better binding profile than the shorter benzoyl chain (e.g., compound **24**, with $K_i hA_3 = 5.24$ nM, $hA_1/hA_3 > 5730$; $hA_{2A}/hA_3 > 19100$). Moreover, the spare H on the nitrogen atom at N⁵ did not seem to be

crucial because its replacement with an additional benzoyl chain (as in compounds **27**, $K_i hA_3 = 6.88$ nM and **28**, $K_i hA_3 = 6.94$ nM), although less favorable than a single chain, still maintained affinity at hA_3 receptor and good selectivity (> 1400) against other receptor subtypes. This finding again confirmed the postulation that the binding pocket of A_3 receptor around this N⁵ position was roomy enough to accommodate the bulky and branched bis-benzamidic substituent; at A_1 and A_{2A} subtypes, there was limited space available for such bulky groups and resulted in decrease of affinity with subsequent increase of selectivity against these two receptors.

N⁸ Position. It was found that when a small alkyl group was present at N⁸, the compounds (**7–12**, **21–28**, and **31–36**) showed a preference for hA_3 receptors, regardless of substitution at N⁵ and C² positions (e.g., compounds **7** [(with a phenyl at C² and a free amino at N⁵), $K_i hA_3 = 75.0$ nM] and **8** [(with a 4-fluorophenyl at C² and a free amino at N⁵), $K_i hA_3 = 31.4$ nM] versus compounds **21** [(with a phenyl at C² and a benzamide at N⁵), $K_i hA_3 = 5.0$ nM] and **22** [(with a 4-fluorophenyl at C² and a benzamide at N⁵), $K_i hA_3 = 3.43$ nM]. This was further confirmed by the introduction of a slightly longer alkyl chain (e.g., an ethyl group in compound **14**, $K_i hA_3 = 68.7$ nM; $hA_1/hA_3 = 22.9$; $hA_{2A}/hA_3 = 12.3$), which still showed hA_3 antagonism and moderate selectivity. Notably, when the same substituent was shifted from position N⁸ to N⁷ (as in compounds **13**, $K_i hA_3 = 565$ nM and **17**, $K_i hA_3 > 30000$ nM), the affinity at hA_3 receptors dropped to at least 8 times, with the resulting binding affinity profile inclined toward hA_{2A} receptors. This observation was substantiated by the results previously reported on N⁷-substituted PTPs as potent hA_{2A} antagonists.³¹

Conversely, when a group bigger than ethyl was introduced at N⁸ (e.g., phenylethyl group in compounds **15**, **16**, **18–20**, and **29**, **30**), a decrease of affinity at hA_3 receptor was observed. In derivatives with free amino group at N⁵ position, the substitution of the methyl group (e.g., compound **11**, $K_i hA_3 = 16.7$ nM) to the long and bulky phenylethyl group (e.g., compound **20**, $K_i hA_3 = 25.0$ nM) only showed a slight decrease of the hA_3 affinity. When a substituent was introduced at the N⁵ position (e.g., compound **29**, $K_i hA_3 = 23.9$ nM), the presence of the phenylethyl group seemed to

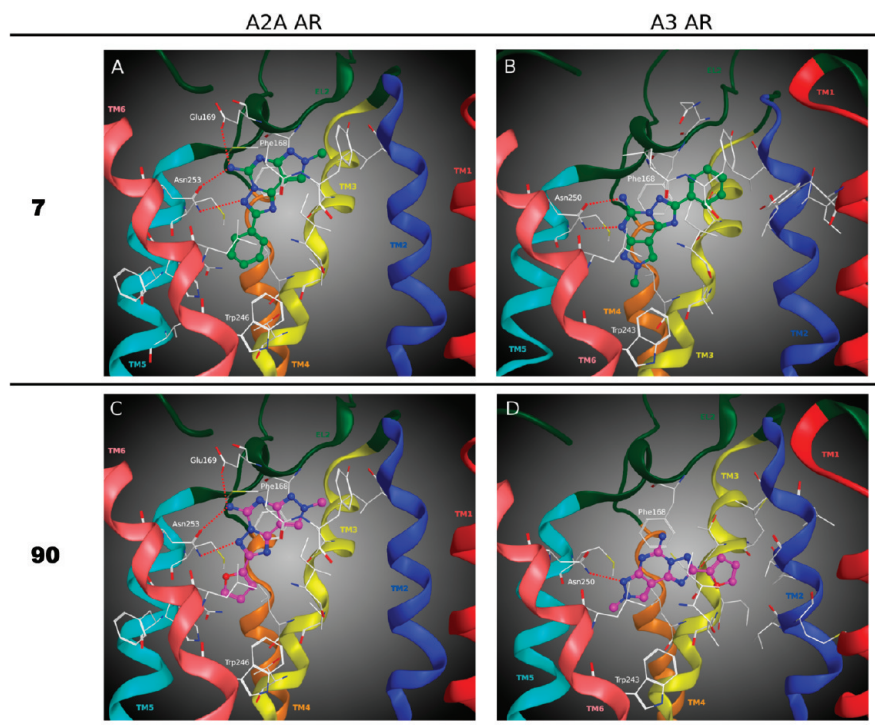


Figure 1. Hypothetical binding modes of the N^5 -unsubstituted derivatives obtained after docking simulations: (A) compound **7** inside the hA_{2A} AR binding site; (B) compound **7** inside the hA_3 AR binding site; (C) compound **90** inside the hA_{2A} AR binding site; (D) compound **90** inside the hA_3 AR binding site. Poses are viewed from the membrane side facing TM6, TM7, and TM1. The view of TM7 is voluntarily omitted. Side chains of some amino acids important for ligand recognition and H-bonding interactions are highlighted. Hydrogen atoms are not displayed.

have resulted in a great decrease of hA_3 affinity in comparison to its N^8 -methyl counterpart (compound **21**, $K_i hA_3 = 5.0$ nM). This might be due to reason that in the N^5 -unsubstituted derivatives, there was still enough space for the bulky phenylethyl group to orientate itself inside the binding cavity. Once an additional group was introduced at the N^5 position, there was limited space remained to anchor the phenylethyl, thus causing a considerable decrease of hA_3 affinity. Apparently, an inverse relationship appeared between the binding affinity values at hA_3 receptor and the molecular volume (MV) of the substituent at position N^8 : the higher the MV, the lower the affinity toward the hA_3 receptor.¹⁰

On the whole, these results confirmed the importance of the contemporary introduction, in the PTP system, of (a) small substituents (e.g., CH_3) at the N^8 position to maintain affinity and selectivity at hA_3 AR, (b) a longer chain such as a phenylacetyl group at the N^5 position to confer higher affinity and a better selectivity especially toward hA_1 and hA_{2A} receptors, (c) a 2-(*para*-substituted) phenyl ring at C^2 to improve affinity and selectivity profile at hA_3 receptors in relative to the 2-furyl counterparts and protect from enzyme deactivation with subsequent higher plasma bioavailability. Among the newly synthesized PTP derivatives, compound **31**, with a phenyl at C^2 , a methyl group at N^8 , and a phenylacetamidic chain at N^5 , showed the best hA_3 affinity profile ($K_i hA_3 = 0.108$ nM) and good selectivity against the other adenosine receptors ($hA_1/hA_3 = 5200$; $hA_{2A}/hA_3 = 7200$).

B. Molecular Modeling Studies. A receptor-driven molecular modeling investigation has been performed in order to rationalize the results obtained from the pharmacological evaluation. For that purpose, we performed molecular

docking simulations on both the crystallographic structure of hA_{2A} ²² and the recently published hA_3 receptor model.^{28,29} All the newly synthesized 2-aryl-PTP derivatives were docked into the orthosteric TMs binding cavities of both adenosine receptors. In addition, docking studies were also performed on the two previously reported PTPs bearing a furan ring at C^2 (compounds **90** and **91** in Table 2),^{10,30} with the aim of comparing the possible differences in binding mode between the 2-aryl and 2-furyl derivatives. On top of that, individual electrostatic contribution (ΔE_{int}^{el}) to the interaction energy (ΔE_{int}) of each receptor residue involved in binding interaction with the ligands (see Supporting Information) was also calculated in order to analyze the ligand–receptor recognition mechanism in a more quantitative manner.

a. N^5 -Unsubstituted Derivatives. From the docking simulation analysis, almost all the new derivatives with free amino group at N^5 (compounds **7–20**) were seen to share a similar binding pose in the TM region of the hA_3 AR. The ligand recognition occurred in the upper region of the TM bundle, and the PTP scaffold was surrounded by TMs 3, 5, 6, and 7 with the 2-aryl ring oriented toward TM2. Figure 1B showed the hypothetical binding pose of compound **7**. This compound was anchored, inside the binding cleft, by two stabilizing hydrogen-bonding interactions with the side chain of Asn250 (6.55), which is highly conserved among all AR subtypes and found to be important for ligand binding at the hA_3 AR.³² It also formed an aromatic π – π stacking interaction with Phe168 (EL2), while the methyl group at N^8 was in proximity with the highly conserved Trp243 (6.48), an important residue in receptor activation and antagonist recognition.³² It was also found to form hydrophobic interactions with many residues of the binding site including

Ala69 (2.61), Val72 (2.64), Thr87 (3.29), Leu90 (3.32), Leu91 (3.33), Phe168 (EL2), Trp243 (6.48), Leu246 (6.51), Leu264 (7.35), Tyr265 (7.36), and Ile268 (7.39). On the other hand, by comparing the binding mode of the 2-furyl counterpart (compound **90** in Table 2) at the hA₃ receptor (Figure 1D), we observed a slight different binding orientation as compared to compound **7**. In fact, this compound was found to be oriented almost parallel to the membrane plane, and it formed only one H-bond with Asn250 (6.55) with concurrent loss of the π - π stacking interaction with Phe168 (EL2).

Through the analysis of electrostatic contributions per residues to the whole interaction energy, we found that Asn250 (6.55) showed a very negative electrostatic interaction energy in complex between compound **7** and hA₃ receptor due to the two stabilizing H-bonding interactions with the ligand (see Supporting Information for details). Conversely, for complex between compound **90** and hA₃ receptor, the same residue showed only a weak stabilizing electrostatic interaction. Therefore, the loss of one H-bond with Asn250 (6.55) and the π - π stacking interaction with Phe168 (EL2) could be the reason to account for the observation that the 2-furyl derivative possessed lower affinity toward the hA₃ receptor as compared to the 2-aryl derivative (compound **7**, K_{ih}A₃ = 75 nM; compound **90**, K_{ih}A₃ = 300 nM).

As regards the compounds with bulkier substituents at N⁸, such as ethyl group (compound **14**) and phenylethyl group (compounds **15–16** and **18–20**), they showed similar binding mode at hA₃ receptor as compared to the N⁸-methyl derivatives. There seemed to be enough space in the binding cavity to accommodate such substituents at this position. Moreover, the presence of different groups at the *para* position of the phenyl ring at C² (e.g., Cl, F, Br, OCH₃) was well tolerated at this receptor with the only exception for the nitro group. Both steric and/or dipolar contributions of nitro group can be responsible for the loss of activity of compound **12**.

In the context of hypothetical binding poses of compound **7** and compound **90** inside the cavity of hA_{2A} receptor (Figure 1, panels A and C, respectively), we noted that they were very similar to each other. In fact, at the hA_{2A} receptor, both compounds formed two H-bonds with Asn253 (6.55) and another H-bond with Glu169 (EL2), in which these two residues have been indicated to play an important role in ligand binding at the hA_{2A} AR.^{33,34} In addition, a π - π stacking interaction with Phe168 (EL2) and hydrophobic interactions with many residues of the binding site including Val84 (3.32), Leu85 (3.33), Thr88 (3.36), Met177 (5.38), Trp246 (6.48), Leu249 (6.51), His250 (6.52), Met270 (7.35), and Ile274 (7.39), were also observed. Two of the strongly negative electrostatic contributions to the interaction energy were found to be related to the Glu169 (EL2) and Asn253 (6.55) for both complexes; however, the contribution due to Glu169 (EL2) was of around -8 kcal/mol for the compound **7**-hA_{2A} AR complex and -14 kcal/mol for the compound **90**-hA_{2A} AR complex. This finding explained why compound **7** still possessed affinity for the hA_{2A} receptor (K_{ih}A_{2A} = 121 nM) but less as compared to the analogue with a 2-furyl ring (compound **90**, K_{ih}A_{2A} = 2.80 nM). Besides that, the presence of substituents at the *para* position of the C²-phenyl ring has imparted a detrimental effect toward the hA_{2A} receptor affinity. With the increase in size of the *para*-substituents, a decrease in affinity at the hA_{2A} receptor was observed, which implied the existence of steric control within

this region of the binding site. Moreover, the substituents at the *para* position of the C²-phenyl ring could affect the approaching of ligands into the hA_{2A} receptor binding cavity and subsequently mediating some interactions with residues at the entrance of the binding site. This step could be crucial for the recognition process and so for ligand affinity at the receptor.³⁵ Therefore, the presence of polar residues at the entrance of the hA_{2A} receptor binding cavity, such as Glu169 (EL2) and His264 (EL3), might affect ligand orientation while approaching the binding pocket, as already proposed.²⁸

As for the N⁷-substituted derivative, it was found that compound **13** showed similar binding mode at both the hA₃ and hA_{2A} receptor subtypes to that of the N⁸-substituted derivatives. Further details on the binding mode of this compound are available in Supporting Information (Figure S1).

b. N⁵-Substituted Derivatives. As shown in Figure 2, the hypothetical binding modes at hA_{2A} and hA₃ receptors for the N⁵-substituted derivatives with a 2-aryl ring (compounds **21–36**) were the same as those obtained for 2-furyl counterpart (compound **91**). For these compounds, recognition at hA₃ receptor occurred in the upper region of the TM bundle, and the PTP scaffold was surrounded by TMs 3, 5, 6, and 7 with the 2-aryl or 2-furyl ring oriented toward TM2 and the substituent at N⁸ located deep into the binding cavity. At the hA₃ receptor, compounds **31** and **91** formed two stabilizing H-bonding interactions with Asn250 (6.55), a π - π stacking interaction between the triazole ring and Phe168 (EL2) and hydrophobic interactions with several residues of the binding site including Ala69 (2.61), Val72 (2.64), Thr87 (3.29), Leu90 (3.32), Leu91 (3.33), Phe168 (EL2), Val169 (EL2), Trp243 (6.48), Leu246 (6.51), Ile249 (6.54), Ile253 (6.58), Val259 (EL3), Leu264 (7.35), Tyr265 (7.36), and Ile268 (7.39) (Figure 2B,D). By analyzing the calculated individual electrostatic contribution to the interaction energy of each receptor residue, it was evident that the Asn250 (6.55) strongly stabilized the ligand-hA₃ receptor complex (negative electrostatic interaction energy) due to the two hydrogen bonding interactions (see Supporting Information).

Considering the hypothetical binding pose of these compounds at the hA_{2A} receptor (Figure 2A,C), it could be seen that the PTP core was rotated of about 40° compared to the binding pose of the same compounds at the hA₃ subtypes. Because of this different orientation of the molecules inside the binding cleft at the hA_{2A} receptor, both compounds **31** and **91** formed only one H-bond with Asn253 (6.55). Coherently, for these complexes, the electrostatic contributions to the interaction energy of Asn253 (6.55) were shown to be weakly stabilizing and no other amino acid with a noteworthy negative electrostatic interaction energy was identified (see Supporting Information).

In fact, it has to be pointed out that at the position 169 (EL2) of the hA₃ receptor subtype, a valine residue is present while at the corresponding position of the hA_{2A} receptor, this valine is replaced by a glutamate residue (Glu169). It was believed that at the hA_{2A} receptor, the substituent at N⁵ of these derivatives were unable to occupy the same position as that of the hA₃ receptor and hence, the whole molecule was shifted away from the Asn253 with a simultaneous loss of a H-bond, as seen in compound **31** at the hA_{2A} binding site. This finding could be accounted for the low affinity profile at the hA_{2A}, as observed in the majority of the N⁵-substituted derivatives (compounds **22–36**). In addition, due to the

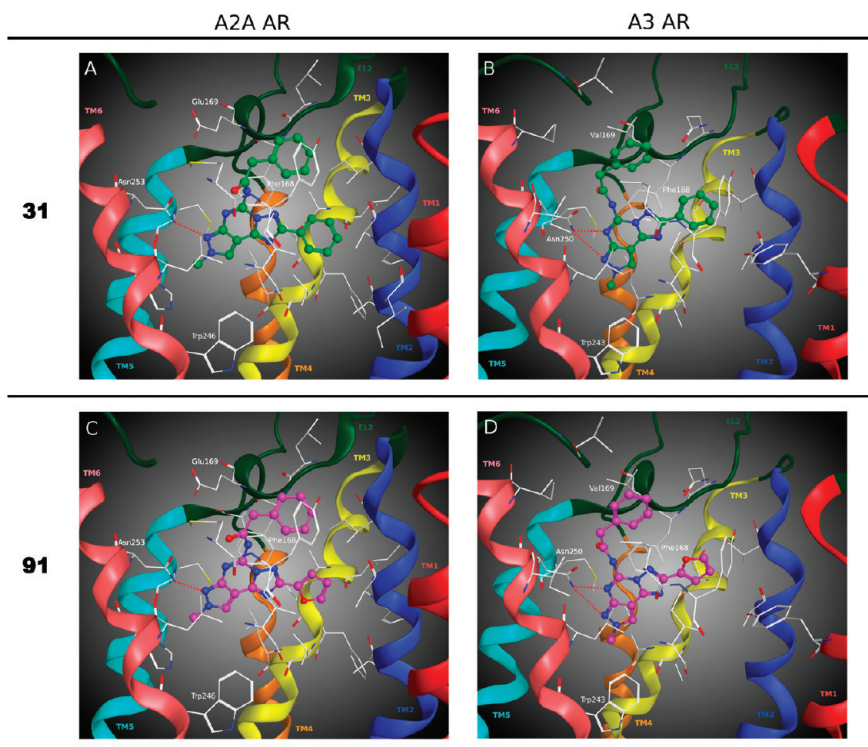


Figure 2. Hypothetical binding modes of the N⁵-substituted derivatives obtained after docking simulations: (A) compound **31** inside the hA_{2A} AR binding site; (B) compound **31** inside the hA₃ AR binding site; (C) compound **91** inside the hA_{2A} AR binding site; (D) compound **91** inside the hA₃ AR binding site. Poses are viewed from the membrane side facing TM6, TM7, and TM1. The view of TM7 is voluntarily omitted. Side chains of some amino acids important for ligand recognition and H-bonding interactions are highlighted. Hydrogen atoms are not displayed.

presence of N⁵-substitutions, these derivatives could not form the H-bonding interactions with Glu169 (EL2) as observed for N⁵-unsubstituted analogues. Therefore, the mutation of the valine at the position 169 with a glutamate was hypothesized to be critical for the hA₃ versus hA_{2A} selectivity profile.²⁸ Moreover, at the hA_{2A} receptor, the hydrophobic side cleft delimited by TM2 and TM3 could well accommodate the 2-furyl ring of compound **91** but hardly accommodated the 2-phenyl ring of compound **31**. This steric effect could be the reason of the difference in affinity between the 2-aryl and the 2-furyl analogues at this receptor subtype (compound **31**, K_{ihA_{2A}} = 778 nM; compound **91**, K_{ihA_{2A}} = 432 nM). For the same reason, the presence of *para*-substituents on the phenyl ring led to a drastic decrease in affinity at hA_{2A} receptor, up to complete loss of affinity for bulkier substituents. Conversely, the 2-phenyl and 2-furyl rings of compounds **31** and **91**, respectively, were located less deeply in the binding cavity of hA₃ receptor and hence, more space was available to accommodate them. Therefore, at the hA₃ receptor subtype, the 2-phenyl ring was preferred, and different *para*-substituents were also well tolerated.

Conclusions

In summary, the bioisosteric replacement of the furan ring with a phenyl ring at the C² position has led to the identification of new series of 2-(*para*-substituted)phenyl-pyrazolo-triazolo-pyrimidine derivatives as hA₃ antagonists with good affinity and remarkably improved selectivity profile toward the other adenosine receptor subtypes in comparison to the 2-furyl PTP derivatives. Moreover, the substitution of 2-furyl with an aryl group in the new PTP derivatives is expected to

overcome the metabolic instability due to the C²-furan ring. Through an additional molecular modeling investigation, the experimental structure–affinity relationship (SAR) findings have been rationalized by depicting the hypothetical binding mode between these newly synthesized derivatives and the specific amino acid residues within the binding site of hA₃ and hA_{2A} receptors. In short, the rational design and synthesis of this new series of 2-(*para*-substituted)phenyl-pyrazolo-triazolo-pyrimidines has given rise to a class of potent, highly selective, and metabolically stable hA₃AR antagonists.

Experimental Section

A. Chemistry. Reactions were routinely monitored by thin-layer chromatography (TLC) on silica gel plate (precoated 60 F₂₅₄ Merck plate). Column chromatographies were performed using silica gel 60 (Merck, 70–230 mesh). Melting points were determined on a Gallenkamp instrument and were uncorrected. Compounds were dissolved in HPLC (high performance liquid chromatography)-grade methanol for determination of mass to charge ratio (*m/z*) via the LCQ Finnigan MAT mass spectrometer (source of ionization: atmospheric pressure chemical ionization (APCI) probe). Purity of compounds was detected by elemental analyses performed at the laboratory of microanalysis of the Department of Chemistry, University of Ferrara (Italy), and all the compounds were confirmed to achieve ≥95% purity. ¹H spectra were determined in deuterated chloroform (CDCl₃) or deuterated dimethylsulfoxide (DMSO-*d*₆) through a Bruker DPX 300 MHz spectrometer, with chemical shifts given in parts per million (δ) downfield relative to the central peak of the solvents, and *J* values (coupling constants) given in hertz. The following abbreviations were used: s, singlet; bs, broad singlet; d, doublet; dd, double doublet; bd, broad doublet; t, triplet; m, multiplet.

General Procedure for the preparation of 2-aryl-8-methylpyrazolo[4,3-*e*]1,2,4-triazolo[1,5-*c*]pyrimidin-5-amines (7–12), 2-(4-Chlorophenyl)-7- or -8-ethyl-pyrazolo[4,3-*e*]1,2,4-triazolo[1,5-*c*]pyrimidin-5-amines (13, 14) and 2-aryl-7- or -8-phenylethyl-pyrazolo[4,3-*e*]1,2,4-triazolo[1,5-*c*]pyrimidin-5-amines (15–20). The 1- and 2-alkyl 5-amino-4-cyano-pyrazole regioisomers (38–42) and corresponding imidates (43–47) for the methyl as well as the ethyl and phenylethyl series were prepared as previously described in refs 23 and 10.

The mixture of imidates (10 mmol) (43–47) were then dissolved in 2-methoxyethanol (50 mL), and (4-substituted)-benzoic hydrazide (13 mmol) was added. The mixture was refluxed for 12 h at 150 °C to afford intermediates 48–61; after cooling, the solvent was removed under reduced pressure and the dark oily residue was cyclized further in diphenyl ether (50 mL) at 260 °C. After 3 h, the mixture was poured onto cold hexane (300 mL). The precipitate was filtered off and purified by chromatography (AcOEt:Petroleum ether in different ratios). The major product, N⁸-substituted compounds, was obtained in good overall yield (60%).

The obtained regioisomers (compounds 62–75) were dissolved in 20 mL of 1,4-dioxane, followed by addition of 5 mL of concentrated hydrochloric acid, 37% w/w into the solution (with final concentration of HCl ~ 20%). The mixture was refluxed for 2 h at 120 °C, and after cooling, the solvent was removed under reduced pressure. The mixture was further basified with saturated sodium bicarbonate and extracted with EtOAc (3 × 50 mL). The organic layers were dried over anhydrous Na₂SO₄ and evaporated under reduced pressure. The residue obtained was crystallized from EtOAc to afford the hydrolyzed compound as solid (76–89); this derivative represented the hydrolyzed form of previous regioisomers, and it was subjected to next step of reaction without further purification.

The hydrolyzed derivatives (76–89) (1 mmol) were subsequently dissolved in 10 mL of 1-methyl-2-pyrrolidinone and cyanamide (12 mmol) was added into the solution, followed by *p*-toluene sulfonic acid monohydrate (3 mmol). The mixture was refluxed for 12 h at 160 °C. The excess of cyanamide was precipitated by addition of 80 mL of EtOAc, followed by filtration and solvent from the filtrate was removed under reduced pressure. A brown-colored mixture consisting of pyrazolo-triazolo-pyrimidines (compounds 7–20) was obtained. The mixture was then purified by column chromatography (AcOEt:petroleum ether in different ratios).

2-(Phenyl)-8-methylpyrazolo[4,3-*e*]1,2,4-triazolo[1,5-*c*]pyrimidin-5-amine (7). Yield 52%, pale-yellow solid, mp 242–244 °C (AcOEt–petroleum ether). ¹H NMR (300 MHz, DMSO-*d*₆) δ: 4.03 (3H, s, Me), 7.56–7.63 (5H, m, NH₂ and aromatic 3H), 8.23 (2H, d, aromatic H, *J* = 8), 8.59 (1H, s, pyrazolo-H). MS-APCI (methanol) *m/z*: 266.0 (M + 1)⁺. Anal. (C₁₃H₁₁N₇) C, H, N.

2-(4-Fluorophenyl)-8-methylpyrazolo[4,3-*e*]1,2,4-triazolo[1,5-*c*]pyrimidin-5-amine (8). Yield 54%, pale-yellow solid, mp > 300 dec °C, (AcOEt–petroleum ether). ¹H NMR (300 MHz, DMSO-*d*₆) δ: 4.02 (3H, s, Me), 7.40 (2H, dd, aromatic H, *J* = 9, *J* = 9), 7.61 (2H, s, NH₂), 8.25 (2H, dd, aromatic H, *J* = 6, *J* = 8), 8.59 (1H, s, pyrazolo-H). MS-APCI (methanol) *m/z*: 284.3 (M + 1)⁺. Anal. (C₁₃H₁₀N₇F) C, H, N.

2-(4-Chlorophenyl)-8-methylpyrazolo[4,3-*e*]1,2,4-triazolo[1,5-*c*]pyrimidin-5-amine (9). Yield 25%, brown solid, mp 177–179 °C, (AcOEt–petroleum ether). ¹H NMR (300 MHz, DMSO-*d*₆) δ: 4.19 (3H, s, Me), 7.62 (2H, s, NH₂), 7.66 (2H, d, aromatic H, *J* = 8), 8.23 (2H, d, aromatic H, *J* = 8), 8.58 (1H, s, pyrazolo-H). MS-APCI (methanol) *m/z*: 299.5 (M + 1)⁺. Anal. (C₁₃H₁₀N₇Cl) C, H, N.

2-(4-Bromophenyl)-8-methylpyrazolo[4,3-*e*]1,2,4-triazolo[1,5-*c*]pyrimidin-5-amine (10). Yield 47%, brown solid, mp > 300 dec °C, (AcOEt–petroleum ether). ¹H NMR (300 MHz, DMSO-*d*₆) δ: 4.21 (3H, s, Me), 7.62 (2H, s, NH₂), 7.89 (2H, d, aromatic H, *J* = 8), 8.12 (2H, d, aromatic H, *J* = 8), 8.29 (1H, s, pyrazolo-H).

MS-APCI (methanol) *m/z*: 345.4 (M + 1)⁺. Anal. (C₁₃H₁₀N₇Br) C, H, N.

2-(4-Methoxyphenyl)-8-methylpyrazolo[4,3-*e*]1,2,4-triazolo[1,5-*c*]pyrimidin-5-amine (11). Yield 54%, mp 313–314 °C (DMF–EtOH). ¹H NMR (300 MHz, DMSO-*d*₆) δ: 3.85 (3H, s, OMe), 4.03 (3H, s, Me), 7.11 (2H, d, aromatic H, *J* = 8.7), 7.57 (2H, s, NH₂), 8.16 (2H, d, aromatic H, *J* = 8.7), 8.57 (1H, s, pyrazolo-H). MS-APCI (methanol) *m/z*: 296.3 (M + 1)⁺. Anal. (C₁₄H₁₃N₇O) C, H, N.

2-(4-Nitrophenyl)-8-methylpyrazolo[4,3-*e*]1,2,4-triazolo[1,5-*c*]pyrimidin-5-amine (12). Yield 53%, mp > 300 dec °C (DMF–EtOH). ¹H NMR (300 MHz, DMSO-*d*₆) δ: 4.04 (3H, s, Me), 7.72 (2H, s, NH₂), 8.43 (2H, d, aromatic H, *J* = 9), 8.47 (2H, d, aromatic H, *J* = 9), 8.63 (1H, s, pyrazolo-H). MS-APCI (methanol) *m/z*: 311.4 (M + 1)⁺. Anal. (C₁₃H₁₀N₈O₂) C, H, N.

2-(4-Chlorophenyl)-7-ethylpyrazolo[4,3-*e*]1,2,4-triazolo[1,5-*c*]pyrimidin-5-amine (13). Yield 35%, pale-yellow solid, mp > 300 dec °C, (AcOEt–petroleum ether). ¹H NMR (300 MHz, CDCl₃) δ: 1.59 (3H, t, CH₃, *J* = 7), 4.61 (2H, q, N⁷-CH₂, *J* = 7), 7.49 (2H, d, aromatic H, *J* = 8), 8.00 (2H, s, NH₂), 8.21–8.31 (3H, m, aromatic 2H and pyrazolo-H). MS-APCI (methanol) *m/z*: 314.2 (M + 1)⁺. Anal. (C₁₄H₁₂N₇Cl) C, H, N.

2-(4-Chlorophenyl)-8-ethylpyrazolo[4,3-*e*]1,2,4-triazolo[1,5-*c*]pyrimidin-5-amine (14). Yield 18%, brown solid, mp > 300 dec °C (AcOEt–petroleum ether). ¹H NMR (300 MHz, DMSO-*d*₆) δ: 1.47 (3H, t, CH₃, *J* = 7), 4.31 (2H, q, N⁸-CH₂, *J* = 7), 7.61 (2H, s, NH₂), 7.67 (2H, d, aromatic H, *J* = 8), 8.22 (2H, d, aromatic H, *J* = 8), 8.61 (1H, s, pyrazolo-H). MS-APCI (methanol) *m/z*: 314.4 (M + 1)⁺. Anal. (C₂₀H₁₆ClN₇) C, H, N.

2-(Phenyl)-8-phenylethylpyrazolo[4,3-*e*]1,2,4-triazolo[1,5-*c*]pyrimidin-5-amine (15). Yield 17%, yellow solid, mp 137–139 °C (AcOEt–petroleum ether). ¹H NMR (300 MHz, DMSO-*d*₆) δ: 3.22 (2H, t, Ph-CH₂, *J* = 7), 4.54 (2H, t, N⁸-CH₂, *J* = 7), 7.16–7.28 (5H, m, aromatic H), 7.55–7.62 (5H, m, NH₂ and aromatic 3H), 8.23–8.26 (2H, d, aromatic H), 8.49 (1H, s, pyrazolo-H). MS-APCI (methanol) *m/z*: 356.5 (M + 1)⁺. Anal. (C₂₀H₁₇N₇) C, H, N.

2-(4-Fluorophenyl)-8-phenylethylpyrazolo[4,3-*e*]1,2,4-triazolo[1,5-*c*]pyrimidin-5-amine (16). Yield 21%, pale-yellow solid, mp 261–263 °C (AcOEt–petroleum ether). ¹H NMR (300 MHz, DMSO-*d*₆) δ: 3.22 (2H, t, Ph-CH₂, *J* = 7), 4.54 (2H, t, N⁸-CH₂, *J* = 7), 7.12–7.28 (5H, m, aromatic H), 7.39 (2H, dd, aromatic H, *J* = 9, *J* = 9), 7.61 (2H, s, NH₂), 8.24 (2H, dd, aromatic H, *J* = 6, *J* = 6), 8.47 (1H, s, pyrazolo-H). MS-APCI (methanol) *m/z*: 374.8 (M + 1)⁺. Anal. (C₂₀H₁₆FN₇) C, H, N.

2-(4-Chlorophenyl)-7-phenylethylpyrazolo[4,3-*e*]1,2,4-triazolo[1,5-*c*]pyrimidin-5-amine (17). Yield 25%, dark-yellow solid, mp 277–279 °C (AcOEt–petroleum ether). ¹H NMR (300 MHz, DMSO-*d*₆) δ: 3.18 (2H, t, Ph-CH₂, *J* = 7), 4.49 (2H, t, N⁸-CH₂, *J* = 7), 7.18–7.26 (5H, m, aromatic H), 7.60 (2H, d, aromatic H, *J* = 8), 8.01 (2H, s, NH₂), 8.14–8.24 (3H, m, aromatic 2H, and pyrazolo-H). MS-APCI (methanol) *m/z*: 390.4 (M + 1)⁺. Anal. (C₂₀H₁₆ClN₇) C, H, N.

2-(4-Chlorophenyl)-8-phenylethylpyrazolo[4,3-*e*]1,2,4-triazolo[1,5-*c*]pyrimidin-5-amine (18). Yield 17%, orange solid, mp 287–289 °C, (AcOEt–petroleum ether). ¹H NMR (300 MHz, DMSO-*d*₆) δ: 3.22 (2H, t, Ph-CH₂, *J* = 7), 4.54 (2H, t, N⁸-CH₂, *J* = 7), 7.18–7.29 (5H, m, aromatic H), 7.62–7.65 (4H, m, NH₂ and aromatic 2H), 8.21 (2H, d, aromatic H, *J* = 8), 8.49 (1H, s, pyrazolo-H). MS-APCI (methanol) *m/z*: 390.7 (M + 1)⁺. Anal. (C₂₀H₁₆ClN₇) C, H, N.

2-(4-Bromophenyl)-8-phenylethylpyrazolo[4,3-*e*]1,2,4-triazolo[1,5-*c*]pyrimidin-5-amine (19). Yield 20%, beige solid, mp 295–297 °C (AcOEt–petroleum ether). ¹H NMR (300 MHz, DMSO-*d*₆) δ: 3.22 (2H, t, Ph-CH₂, *J* = 7), 4.54 (2H, t, N⁸-CH₂, *J* = 7), 7.18–7.29 (5H, m, aromatic H), 7.65 (2H, s, NH₂), 7.77 (2H, d, aromatic H, *J* = 8), 8.14 (2H, d, aromatic H, *J* = 8), 8.48 (1H, s, pyrazolo-H). MS-APCI (methanol) *m/z*: 434.6 (M + 1)⁺. Anal. (C₂₀H₁₆BrN₇) C, H, N.

2-(4-Methoxyphenyl)-8-phenylethylpyrazolo[4,3-*e*]1,2,4-triazolo[1,5-*c*]pyrimidin-5-amine (20). Yield 15%, pale-yellow solid, mp 217–219 °C (AcOEt–petroleum ether). ¹H NMR (300 MHz, DMSO-*d*₆) δ: 3.22 (2H, t, Ph-CH₂, *J* = 7), 3.84 (3H, s, CH₃), 4.54 (2H, t, N⁸-CH₂, *J* = 7), 7.10 (2H, d, aromatic H, *J* = 9), 7.13–7.26 (5H, m, aromatic H), 7.58 (2H, s, NH₂), 8.14 (2H, d, aromatic H, *J* = 9), 8.46 (1H, s, pyrazolo-H). MS-APCI (methanol) *m/z*: 386.8 (M + 1)⁺. Anal. (C₂₁H₁₉N₇O) C, H, N.

General Procedure for *N*-(2-Aryl-8-methylpyrazolo[4,3-*e*]-[1,2,4]triazolo[1,5-*c*]pyrimidin-5-yl)benzamide (21–26). To a suspension of 0.3 mmol of 2-aryl-8-methylpyrazolo[4,3-*e*]-[1,2,4]triazolo[1,5-*c*]pyrimidin-5-amine (7–12) in 10 mL of toluene, 0.27 g (1.2 mmol) of benzoic anhydride was added. The mixture was heated under reflux and stirred for 6–12 h. The solvent was removed under reduced pressure, and the residue was crystallized from an appropriate solvent.

***N*-[2-(Phenyl)-8-methylpyrazolo[4,3-*e*][1,2,4]triazolo[1,5-*c*]pyrimidin-5-yl]benzamide (21).** Yield 53%, pale-yellow solid, mp 265–267 °C (AcOEt–petroleum ether). ¹H NMR (300 MHz, CDCl₃) δ: 4.21 (3H, s, Me), 7.43–7.72 (6H, m, aromatic H), 8.08–8.15 (2H, bd, aromatic H), 8.25 (1H, s, pyrazolo-H), 8.27–8.38 (2H, bd, aromatic H), 9.84 (1H, s, NH). MS-APCI (methanol) *m/z*: 370.2 (M + 1)⁺. Anal. (C₂₀H₁₅N₇O) C, H, N.

***N*-[2-(4-Fluorophenyl)-8-methylpyrazolo[4,3-*e*][1,2,4]triazolo[1,5-*c*]pyrimidin-5-yl]benzamide (22).** Yield 77%, mp 270–272 °C (EtOH). ¹H NMR (300 MHz, DMSO-*d*₆) δ: 4.20 (3H, s, Me), 7.37 (2H, dd, aromatic H, *J* = 9, *J* = 9), 7.62 (2H, t, aromatic H, *J* = 7), 7.71 (1H, t, aromatic H, *J* = 7), 8.08 (2H, d, aromatic H, *J* = 7), 8.22 (2H, dd, aromatic H, *J* = 6, *J* = 9), 8.93 (1H, s, pyrazolo-H), 11.48 (1H, s, NH). MS-APCI (methanol) *m/z*: 388.3 (M + 1)⁺. Anal. (C₂₀H₁₄FN₇O) C, H, N.

***N*-[2-(4-Chlorophenyl)-8-methylpyrazolo[4,3-*e*][1,2,4]triazolo[1,5-*c*]pyrimidin-5-yl]benzamide (23).** Yield 54%, mp 296–297 °C (MeOH). ¹H NMR (300 MHz, DMSO-*d*₆) δ: 4.20 (3H, s, Me), 7.61 (2H, d, aromatic H, *J* = 9), 7.62 (2H, t, aromatic H, *J* = 7), 7.71 (1H, t, aromatic H, *J* = 7), 8.08 (2H, d, aromatic H, *J* = 7), 8.18 (2H, d, aromatic H, *J* = 9), 8.93 (1H, s, pyrazolo-H), 11.48 (1H, s, NH). MS-APCI (methanol) *m/z*: 404.2 (M + 1)⁺. Anal. (C₂₀H₁₄ClN₇O) C, H, N.

***N*-[2-(4-Bromophenyl)-8-methylpyrazolo[4,3-*e*][1,2,4]triazolo[1,5-*c*]pyrimidin-5-yl]benzamide (24).** Yield 73%, mp 292–294 °C (EtOH). ¹H NMR (300 MHz, DMSO-*d*₆) δ: 4.20 (3H, s, Me), 7.62 (2H, t, aromatic H, *J* = 8), 7.71 (1H, t, aromatic H, *J* = 7), 7.75 (2H, d, aromatic H, *J* = 8), 8.08 (2H, d, aromatic H, *J* = 7), 8.11 (2H, d, aromatic H, *J* = 8), 8.93 (1H, s, pyrazolo-H), 11.50 (1H, s, NH). MS-APCI (methanol) *m/z*: 449.4 (M + 1)⁺. Anal. (C₂₀H₁₄BrN₇O) C, H, N.

***N*-[2-(4-Methoxyphenyl)-8-methylpyrazolo[4,3-*e*][1,2,4]triazolo[1,5-*c*]pyrimidin-5-yl]benzamide (25).** Yield 74%, mp 295–296 °C (EtOH). ¹H NMR (300 MHz, DMSO-*d*₆) δ: 3.83 (3H, s, OMe), 4.20 (3H, s, Me), 7.09 (2H, d, aromatic H, *J* = 9), 7.62 (2H, t, aromatic H, *J* = 7), 7.71 (1H, t, aromatic H, *J* = 8), 8.08 (2H, d, aromatic H, *J* = 7), 8.11 (2H, d, aromatic H, *J* = 9), 8.91 (1H, s, pyrazolo-H), 11.42 (1H, s, NH). MS-APCI (methanol) *m/z*: 400.5 (M + 1)⁺. Anal. (C₂₁H₁₇N₇O₂) C, H, N.

***N*-[2-(4-Nitrophenyl)-8-methylpyrazolo[4,3-*e*][1,2,4]triazolo[1,5-*c*]pyrimidin-5-yl]benzamide (26).** Yield 47%, mp 295–296 °C (EtOH). ¹H NMR (300 MHz, DMSO-*d*₆) δ: 4.20 (3H, s, Me), 7.61 (2H, t, aromatic H, *J* = 8), 7.70 (1H, t, aromatic H, *J* = 7), 8.10 (2H, d, aromatic H, *J* = 8), 8.39 (2H, d, aromatic H, *J* = 9), 8.43 (2H, d, aromatic H, *J* = 9), 8.94 (1H, s, pyrazolo-H), 11.57 (1H, bs, NH₂). MS-APCI (methanol) *m/z*: 414.3 (M + 1)⁺. Anal. (C₂₀H₁₄N₈O₃) C, H, N.

General Procedure for *N*-Benzoyl-*N*-(2-aryl-8-methylpyrazolo[4,3-*e*][1,2,4]triazolo[1,5-*c*]pyrimidin-5-yl)benzamide (27–28). To a suspension of 0.3 mmol of 2-(4-methoxyphenyl)-8-methylpyrazolo[4,3-*e*][1,2,4]triazolo[1,5-*c*]pyrimidin-5-amine (11) in 5 mL of toluene, 0.35 mL (3.0 mmol) of benzoyl chloride was added followed by DIPEA (0.52 mL, 3.0 mmol). The mixture was heated under reflux with stirring for 8 h. The solvent was removed

under reduced pressure, and the bis-acylated product, 27 was later crystallized from EtOH. For the synthesis of 28, the same procedure was followed, with the exceptions that 0.3 mmol of 2-(4-chloro)phenyl-8-methylpyrazolo[4,3-*e*][1,2,4]triazolo[1,5-*c*]pyrimidin-5-amine (9) were suspended in 5 mL of dioxan in the presence of TEA (0.42 mL, 3.0 mmol), and finally the bis-acylated product was crystallized from the MeOH.

***N*-Benzoyl-*N*-[8-methyl-2-(4-methoxyphenyl)-8H-pyrazolo[4,3-*e*][1,2,4]triazolo[1,5-*c*]pyrimidin-5-yl]benzamide (27).** Yield 93%, mp 248–250 °C (EtOH). ¹H NMR (300 MHz, DMSO-*d*₆) δ: 3.81 (3H, s, OMe), 4.15 (3H, s, Me), 7.08 (2H, d, aromatic H, *J* = 9), 7.52 (4H, t, aromatic H, *J* = 8), 7.64 (2H, t, aromatic H, *J* = 7), 7.88 (4H, d, aromatic H, *J* = 8), 8.00 (2H, d, aromatic H, *J* = 9), 8.96 (1H, s, pyrazolo-H). MS-APCI (methanol) *m/z*: 504.4 (M + 1)⁺. Anal. (C₂₈H₂₁N₇O₃) C, H, N.

***N*-Benzoyl-*N*-[8-methyl-2-(4-chlorophenyl)-8H-pyrazolo[4,3-*e*][1,2,4]triazolo[1,5-*c*]pyrimidin-5-yl]benzamide (28).** Yield 50%, mp 278–280 °C (MeOH). ¹H NMR (300 MHz, DMSO-*d*₆) δ: 4.15 (3H, s, Me), 7.51 (4H, t, aromatic H, *J* = 7), 7.58–7.69 (4H, m, aromatic H), 7.89 (4H, d, aromatic H, *J* = 7), 8.08 (2H, d, aromatic H, *J* = 9), 8.99 (1H, s, pyrazolo-H). MS-APCI (methanol) *m/z*: 508.2 (M + 1)⁺. Anal. (C₂₇H₁₈ClN₇O₂) C, H, N.

General Procedure for *N*-(2-Aryl-8-phenylethylpyrazolo[4,3-*e*][1,2,4]triazolo[1,5-*c*]pyrimidin-5-yl)benzamide (29–30). To a suspension of 1 mmol of 2-aryl-8-phenylethylpyrazolo[4,3-*e*][1,2,4]triazolo[1,5-*c*]pyrimidin-5-amine (15, 19) in 10 mL of toluene, 1.81 g (8 mmol) of benzoic anhydride was added. The mixture was refluxed and stirred for 12 h at 120 °C. Then the solvent was removed under reduced pressure and the residue was purified via column chromatography (AcOEt–petroleum ether in different ratios) to obtain the pure N⁵ substituted pyrazolo-triazolo-pyrimidine derivatives (29 and 30).

***N*-[2-(Phenyl)-8-phenylethyl-pyrazolo[4,3-*e*][1,2,4]triazolo[1,5-*c*]pyrimidin-5-yl]benzamide (29).** Yield 27%, light-yellow solid, mp 122–124 °C (AcOEt–petroleum ether). ¹H NMR (300 MHz, CDCl₃) δ: 3.34 (2H, t, Ph-CH₂, *J* = 7), 4.62 (2H, t, N⁸-CH₂, *J* = 7), 7.06–7.22 (5H, m, aromatic H), 7.52–7.68 (6H, m, aromatic H), 7.96 (1H, s, pyrazolo-H), 8.08 (2H, d, aromatic H, *J* = 7), 8.26–8.27 (2H, bd, aromatic H), 9.85 (1H, s, NH). MS-APCI (methanol) *m/z*: 457.7 (M – 1)⁺. Anal. (C₂₇H₂₁N₇O) C, H, N.

***N*-[2-(4-Bromophenyl)-8-phenylethyl-pyrazolo[4,3-*e*][1,2,4]triazolo[1,5-*c*]pyrimidin-5-yl]benzamide (30).** Yield 62%, light-yellow solid, mp 237–239 °C (AcOEt–petroleum ether). ¹H NMR (300 MHz, CDCl₃) δ: 3.34 (2H, t, Ph-CH₂, *J* = 7), 4.62 (2H, t, N⁸-CH₂, *J* = 7), 7.06–7.25 (5H, m, aromatic H), 7.58–7.68 (5H, m, aromatic H), 7.95 (1H, s, pyrazolo-H), 8.08 (2H, d, aromatic H, *J* = 6), 8.14 (2H, d, aromatic H, *J* = 8), 9.80 (1H, bs, NH). MS-APCI (methanol) *m/z*: 539.0 (M + 2)⁺. Anal. (C₂₇H₂₀BrN₇O) C, H, N.

General Procedure for *N*-(2-Aryl-8-methylpyrazolo[4,3-*e*][1,2,4]triazolo[1,5-*c*]pyrimidin-5-yl)phenylacetamide (31–36). To a suspension of 0.3 mmol of 2-aryl-8-methylpyrazolo[4,3-*e*][1,2,4]triazolo[1,5-*c*]pyrimidin-5-amine (7–12) in 15 mL of toluene, 0.16 mL (1.2 mmol) of phenylacetyl chloride was added followed by 0.2–0.5 mL (1.2–3 mmol) of DIPEA. The mixture was heated under reflux with stirring for 6–12 h. The solvent was removed under reduced pressure, and the residue was crystallized from an appropriate solvent.

***N*-[2-(Phenyl)-8-methylpyrazolo[4,3-*e*][1,2,4]triazolo[1,5-*c*]pyrimidin-5-yl]phenylacetamide (31).** Yield 50%, pale-yellow solid, mp 283–285 °C (AcOEt–petroleum ether). ¹H NMR (300 MHz, DMSO-*d*₆) δ: 4.03 (2H, s, CH₂), 4.15 (3H, s, Me), 7.28–7.46 (5H, m, aromatic H), 7.57–7.59 (3H, m, aromatic H), 8.20–8.23 (2H, m, aromatic H), 8.83 (1H, s, pyrazolo-H), 10.90 (1H, bs, NH). MS-APCI (methanol) *m/z*: 384.3 (M + 1)⁺. Anal. (C₂₁H₁₇N₇O) C, H, N.

***N*-[2-(4-Fluorophenyl)-8-methylpyrazolo[4,3-*e*][1,2,4]triazolo[1,5-*c*]pyrimidin-5-yl]phenylacetamide (32).** Yield 38%, mp 229–231 °C (MeOH). ¹H NMR (300 MHz, DMSO-*d*₆) δ: 4.03 (2H, s,

CH₂), 4.16 (3H, s, Me), 7.03 (1H, t, aromatic H, *J* = 7.0), 7.35–7.49 (6H, m, aromatic H), 8.25 (2H, dd, aromatic H, *J* = 6, *J* = 9), 8.84 (1H, s, pyrazolo-H), 10.90 (1H, s, NH). MS-APCI (methanol) *m/z*: 402.4 (M + 1)⁺. Anal. (C₂₁H₁₆FN₇O) C, H, N.

N-[2-(4-Chlorophenyl)-8-methylpyrazolo[4,3-*e*][1,2,4]triazolo-[1,5-*c*]pyrimidin-5-yl]phenylacetamide (33). Yield 36%, mp 223–225 °C (EtOH). ¹H NMR (300 MHz, DMSO-*d*₆) δ: 4.03 (2H, s, CH₂), 4.16 (3H, s, Me), 7.31 (1H, t, aromatic H, *J* = 7), 7.38 (2H, t, aromatic H, *J* = 7), 7.45 (2H, d, aromatic H, *J* = 8), 7.66 (2H, d, aromatic H, *J* = 9), 8.21 (2H, d, aromatic H, *J* = 9), 8.84 (1H, s, pyrazolo-H), 10.93 (1H, s, NH). MS-APCI (methanol) *m/z*: 418.4 (M + 1)⁺. Anal. (C₂₁H₁₆ClN₇O) C, H, N.

N-[2-(4-Bromophenyl)-8-methylpyrazolo[4,3-*e*][1,2,4]triazolo-[1,5-*c*]pyrimidin-5-yl]phenylacetamide (34). Yield 63%, mp 217–218 °C (MeOH). ¹H NMR (300 MHz, DMSO-*d*₆) δ: 4.03 (2H, s, CH₂), 4.16 (3H, s, Me), 7.31 (1H, t, aromatic H, *J* = 7), 7.38 (2H, t, aromatic H, *J* = 7), 7.45 (2H, d, aromatic H, *J* = 8), 7.80 (2H, d, aromatic H, *J* = 9), 8.14 (2H, d, aromatic H, *J* = 9), 8.84 (1H, s, pyrazolo-H), 10.93 (1H, s, NH). MS-APCI (methanol) *m/z*: 463.3 (M + 1)⁺. Anal. (C₂₁H₁₆BrN₇O) C, H, N.

N-[2-(4-Methoxyphenyl)-8-methylpyrazolo[4,3-*e*][1,2,4]triazolo-[1,5-*c*]pyrimidin-5-yl]phenylacetamide (35). Yield 52%, mp 225–226 °C (EtOH). ¹H NMR (300 MHz, DMSO-*d*₆) δ: 3.86 (3H, s, OMe), 4.03 (2H, s, CH₂), 4.15 (3H, s, Me), 7.13 (2H, d, aromatic H, *J* = 9), 7.31 (1H, t, aromatic H, *J* = 7), 7.39 (2H, t, aromatic H, *J* = 7), 7.45 (2H, d, aromatic H, *J* = 7), 8.15 (2H, d, aromatic H, *J* = 9), 8.82 (1H, s, pyrazolo-H), 10.83 (1H, s, NH). MS-APCI (methanol) *m/z*: 413.2 (M + 1)⁺. Anal. (C₂₂H₁₉N₇O₂) C, H, N.

N-[2-(4-Nitrophenyl)-8-methylpyrazolo[4,3-*e*][1,2,4]triazolo-[1,5-*c*]pyrimidin-5-yl]phenylacetamide (36). Yield 57%, mp 248–249 °C (MeOH). ¹H NMR (300 MHz, DMSO-*d*₆) δ: 4.04 (2H, s, CH₂), 4.17 (3H, s, Me), 7.32 (1H, t, aromatic H, *J* = 7), 7.40 (2H, t, aromatic H, *J* = 7), 7.45 (2H, d, aromatic H, *J* = 7), 8.45 (4H, s, aromatic H), 8.88 (1H, s, pyrazolo-H), 11.02 (1H, s, NH). MS-APCI (methanol) *m/z*: 429.4 (M + 1)⁺. Anal. (C₂₁H₁₆N₈O₃) C, H, N.

B. Biology. CHO Membrane Preparation. All the pharmacological methods involving in membrane preparation for radioligand binding experiments followed the procedures as described earlier.²⁴

Membranes for radioligand binding were prepared from cells stably transfected with the human adenosine receptor subtypes (A₁, A_{2A}, and A₃ expressed on CHO cells) in a two-step procedure. In the first low-speed step (1000g for 4 min), the cell fragments and nuclei were removed. After that, the crude membrane fraction was sedimented from the supernatant at 100000g for 30 min. The membrane pellet was then resuspended in the specific buffer used for the respective binding experiments, frozen in liquid nitrogen, and stored at –80 °C. For the measurement of the adenylyl cyclase activity in A_{2B} receptor expressed on CHO cells, only one step of centrifugation was used in which the homogenate was sedimented for 30 min at 54000g. The resulting crude membrane pellet was resuspended in 50 mM Tris/HCl, pH 7.4 and immediately used for the adenylyl cyclase assay.

1. Human Cloned A₁, A_{2A}, A₃ Adenosine Receptor Binding Assay. Binding of [³H]-CCPA to CHO cells transfected with the human recombinant A₁ adenosine receptor was performed as previously described.^{24,25} Displacement experiments were performed for 3h at 25 °C in 200 μL of buffer containing 1 nM [³H]CCPA, 0.2 U/mL adenosine deaminase, 20 μg of membrane protein in 50 mM Tris/HCl, pH 7.4 and tested compound in different concentrations. Nonspecific binding was determined in the presence of 1 mM theophylline.²⁶

Binding of [³H]-NECA to CHO cells transfected with the human recombinant A_{2A} adenosine receptors was performed following the conditions as that described for the A₁ receptor binding.^{24,25} In the displacement experiments, samples containing a protein concentration of 50 μg, 30 nM [³H]-NECA and tested compound in different concentrations were incubated for

3h at 25 °C. Nonspecific binding was determined in the presence of 100 μM R-PIA (R-N⁶-phenylisopropyladenosine).²⁶

Binding of [³H]-NECA to CHO cells transfected with the human recombinant A₃ adenosine receptors was carried out as previously described.^{24,25} The displacement experiments were performed for 3h at 25 °C in buffer solution containing 10 nM [³H]-NECA, 20 μg membrane protein in 50 mM Tris-HCl, 1 mM EDTA (ethylenediaminetetraacetate), 10 mM MgCl₂, pH 8.25 and tested compound in different concentrations. Nonspecific binding was determined in the presence of 100 μM R-PIA.²⁶

Bound and free radioactivity was separated by filtering the assay mixture through Whatman GF/B glass-fiber filters using a Micro-Mate 196-cell harvester (Packard Instrument Company). The filter bound radioactivity was counted on Top Count (efficiency of 57%) with Micro-Scint 20. The protein concentration was determined according to the Bio-Rad method³⁶ with bovine albumin as a reference standard.

2. Adenylyl Cyclase Activity. Because of the lack of a suitable radioligand for hA_{2B} receptor in binding assay, the potency of antagonists at A_{2B} receptor (expressed on CHO cells) was determined in adenylyl cyclase experiments instead. The procedure was carried out as described previously with minor modifications.^{24,25} Membranes were incubated with about 150000 cpm of [α-³²P]ATP for 20 min in the incubation mixture as described^{24,25} without EGTA and NaCl. For agonists, the EC₅₀ values for the stimulation of adenylyl cyclase were calculated with the Hill equation. Hill coefficients in all experiments were near unity. IC₅₀ values for concentration-dependent inhibition of NECA-stimulated adenylyl cyclase caused by antagonists were calculated accordingly. Dissociation constants (*K*_i) for antagonism were then calculated from the Cheng and Prusoff equation.²⁷

C. Molecular Modeling. All modeling studies were carried out on a 20 CPU (Intel Core2 Quad CPU 2.40 GHz) Linux cluster. Homology modeling, energy calculation, and analyses of docking poses were performed using the Molecular Operating Environment (MOE, version 2008.10) suite.³⁷ The software package MOPAC (version 7),³⁸ implemented in MOE suite, was utilized for all quantum mechanical calculations. Docking simulations were performed using GOLD suite.³⁹

1. Homology Models of hA₃AR. On the basis of the assumption that GPCRs share similar TM boundaries and overall topology, a homology model of the hA₃ adenosine receptor was constructed, as previously reported,^{28,29} based on a template of the recently published crystal structure of hA_{2A} receptor (PDB code: 3EML).²²

The numbering of the amino acids follows the arbitrary scheme by Ballesteros and Weinstein. According to this scheme, each amino acid identifier starts with the helix number, followed by the position relative to a reference residue among the most conserved amino acid in that helix. The number 50 is arbitrarily assigned to the reference residue.⁴⁰

First, the amino acid sequences of TM helices of the hA₃ receptor were aligned with those of the template, guided by the highly conserved amino acid residues, including the DRY motif (Asp3.49, Arg3.50, and Tyr3.51) and three proline residues (Pro4.60, Pro6.50, and Pro7.50) in the TM segments of GPCRs. The same boundaries were applied for the TM helices of hA₃ receptor as they were identified from the 3D structure for the corresponding sequences of the template, the coordinates of which were used to construct the seven TM helices for hA₃ receptor. Then, the loop domains were constructed by the loop search method implemented in MOE on the basis of the structure of compatible fragments found in the Protein Data Bank. In particular, loops were modeled first in random order. For each loop, a contact energy function analyzed the list of candidates collected in the segment searching stage, taking into account all atoms already modeled and any atoms specified by the user as belonging to the model environment. These energies were then used to make a Boltzmann-weighted choice from the

candidates, the coordinates of which were then copied to the model. Subsequently, the side chains were modeled using a library of rotamers generated by systematic clustering of the Protein Data Bank data, using the same procedure. Side chains belonging to residues whose backbone coordinates were copied from a template were modeled first, followed by side chains of modeled loops. Outgaps and their side chains were modeled last. Special caution has to be given to EL2 because amino acids of this loop could be involved in direct interactions with the ligands. A driving force to the peculiar fold of the EL2 loop might be the presence of a disulfide bridge between cysteines in TM3 and EL2. Because this covalent link is conserved in both hA_{2A} and hA₃ receptors, the EL2 loop was modeled using a constrained geometry around the EL2–TM3 disulfide bridge. The constraints were applied before the construction of the homology model, in particular during the sequences alignment, selecting the cysteine residues involved in the disulfide bridge in hA_{2A} to be constrained with the corresponding cysteine residues in hA₃ sequence. In particular, Cys166 (EL2) and Cys77 (3.25) of the hA_{2A} receptor were constrained, respectively, with Cys166 (EL2) and Cys83 (3.25) of the hA₃ receptor. During the alignment, MOE-Align attempted to minimize the number of constraint violations. Then, after running the homology modeling, the presence of the conserved disulfide bridge in the model was manually checked. After the heavy atoms were modeled, all hydrogen atoms were added using the Protonate 3D methodology,⁴¹ part of the MOE suite. This application assigned a protonation state for each chemical groups that minimized the total free energy of the system (taking titration into account).⁴¹

Protein stereochemistry evaluation was then performed by several tools (Ramachandran plot; backbone bond lengths, angles and dihedral plots; clash contacts report; rotamers strain energy report) implemented in MOE suite.³⁷

2. Molecular Docking of hA₃AR Antagonists. Ligand structures were built using MOE-builder tool, part of the MOE suite,³⁷ and were subjected to MMFF94x energy minimization until the rms of conjugate gradient was < 0.05 kcal mol⁻¹ Å⁻¹. Partial charges for the ligands were calculated using PM3/ESP methodology.

Four different programs have been used to calibrate our docking protocols: MOE-Dock,³⁷ GOLD,³⁹ Glide,⁴² and PLANTS.⁴³ In particular, ZM-241385 was redocked into the crystal structure of the hA_{2A} adenosine receptor (PDB code: 3EML) with different docking algorithms and scoring functions, as already described.^{28,29} Then, rmsd values between predicted and crystallographic positions of ZM-241385 were calculated for each of the docking algorithms. The results showed that docking simulations performed with GOLD gave the lowest rmsd value, the lowest mean rmsd value and the highest number of poses with rmsd value < 2.5 Å.

On the basis of the best docking performance, all antagonist structures were docked into the hypothetical TM binding site of the hA₃ AR model and that of the hA_{2A} AR crystal structure by using the docking tool of the GOLD suite.³⁹ Searching was conducted within a user-specified docking sphere, using the Genetic Algorithm protocol and the GoldScore scoring function. GOLD performed a user-specified number of independent docking runs (25 in our specific case) and wrote the resulting conformations and their energies in a molecular database file. The resulting docked complexes were subjected to MMFF94x energy minimization until the rms of conjugate gradient was < 0.1 kcal mol⁻¹ Å⁻¹. Charges for the ligands were imported from the MOPAC output files using PM3/ESP methodology.

Prediction of antagonist–receptor complex stability (in terms of corresponding pK_i value) and the quantitative analysis for nonbonded intermolecular interactions (H-bonds, transition metal, water bridges, hydrophobic, electrostatic) were calculated and visualized using several tools implemented in MOE suite.³⁷ Electrostatic contributions to the binding energy of

individual amino acids have been calculated as implemented in MOE suite.³⁷ To estimate the electrostatic contributions, atomic charges for the ligands were calculated using PM3/ESP methodology. Partial charges for protein amino acids were calculated on the basis of the AMBER99 force field.

Acknowledgment. This work has been supported by the National Medical Research Council, Singapore (NMRC/NIG/0020/2008), and the National University of Singapore (R-148-050-091-101/133).

Supporting Information Available: Electrostatic interaction energy between the ligand and individual amino acid involved in ligand recognition of compounds **7**, **31**, **90**, **91**; binding mode of compound **13** inside the hA₃ and hA_{2A} receptors and combustion analysis data of the synthesized compounds. This material is available free of charge via the Internet at <http://pubs.acs.org>.

References

- (1) Linden, J. Cloned adenosine A₃ receptors: pharmacological properties, species differences and receptor functions. *Trends Pharmacol. Sci.* **1994**, *15*, 298–306.
- (2) Jeffe, F.; Stegmann, K. A.; Broelsch, F.; Manns, M. P.; Cornberg, M.; Wedemeyer, H. Adenosine and IFN-α synergistically increase IFN-γ production of human NK cells. *J. Leukocyte Biol.* **2009**, *85*, 452–461.
- (3) Jacobson, K. A. A₃ adenosine receptors: novel ligands and paradoxical effects. *Trends Pharmacol. Sci.* **1998**, *19*, 184–191.
- (4) Gessi, S.; Cattabriga, E.; Avitabile, A.; Gafa', G.; Lanza, G.; Cavazzini, L.; Bianchi, N.; Gambari, R.; Feo, C.; Liboni, A.; Gullini, S.; Leung, E.; Mac-Lennan, S.; Borea, P. A. Elevated Expression of A₃ Adenosine Receptors in Human Colorectal Cancer Is Reflected in Peripheral Blood Cells. *Clin. Cancer Res.* **2004**, *10*, 5895–5901.
- (5) Sajjadi, F. G.; Firestein, G. S. cDNA cloning and sequence analysis of the human A₃ adenosine receptor. *Biochim. Biophys. Acta* **1993**, *1179*, 105–107.
- (6) Salvatore, C. A.; Jacobson, M. A.; Taylor, H. E.; Linden, J.; Johnson, R. G. Molecular cloning and characterization of the human A₃ adenosine receptor. *Proc. Natl. Acad. Sci. U.S.A.* **1993**, *90*, 10365–10369.
- (7) Baraldi, P. G.; Cacciari, B.; Romagnoli, R.; Borea, P. A.; Varani, K.; Pastorin, G.; Da Ros, T.; Tabrizi, M. A.; Fruttarolo, F.; Spalluto, G. Pyrazolo-triazolo-pyrimidine derivatives as adenosine receptor antagonists: a possible template for adenosine receptor subtypes? *Curr. Pharm. Design* **2002**, *8*, 2299–2332.
- (8) Baraldi, P. G.; Cacciari, B.; Romagnoli, R.; Klotz, K. N.; Spalluto, G.; Varani, K.; Gessi, S.; Merighi, S.; Borea, P. A. Pyrazolo[4,3-*e*]1,2,4-triazolo[1,5-*c*]pyrimidine derivatives as adenosine receptor ligands: a starting point for selective A_{2B} adenosine receptor antagonists. *Drug Dev. Res.* **2001**, *53*, 225–235.
- (9) Kim, Y.-C.; Ji, X.-D.; Jacobson, K. A. Derivatives of the Triazoloquinazoline Adenosine Antagonist (CGS15943) Are Selective for the Human A₃ Receptor Subtype. *J. Med. Chem.* **1996**, *39*, 4142–4148.
- (10) Baraldi, P. G.; Cacciari, B.; Romagnoli, R.; Spalluto, G.; Moro, S.; Klotz, K. N.; Leung, E.; Varani, K.; Gessi, S.; Merighi, S.; Borea, P. A. Pyrazolo[4,3-*e*]1,2,4-triazolo[1,5-*c*]pyrimidine Derivatives as Highly Potent and Selective Human A₃ Adenosine Receptor Antagonists: Influence of the Chain at the N⁸ Pyrazole Nitrogen. *J. Med. Chem.* **2000**, *43*, 4768–4780.
- (11) Pastorin, G.; Da Ros, T.; Spalluto, G.; Deflorian, F.; Moro, S.; Cacciari, B.; Baraldi, P. G.; Gessi, S.; Varani, K.; Borea, P. A. Pyrazolo[4,3-*e*]1,2,4-triazolo[1,5-*c*]pyrimidine derivatives as adenosine receptor antagonists. Influence of the N5 substituent on the affinity at the human A₃ and A_{2B} adenosine receptor subtypes: a molecular modeling investigation. *J. Med. Chem.* **2003**, *46*, 4287–4296.
- (12) Maconi, A.; Pastorin, G.; Da Ros, T.; Spalluto, G.; Gao, Z. G.; Jacobson, K. A.; Baraldi, P. G.; Cacciari, B.; Varani, K.; Borea, P. A. Synthesis, biological properties and molecular modeling investigation of the first potent, selective and water soluble human A₃ adenosine receptor antagonist. *J. Med. Chem.* **2002**, *45*, 3579–3582.
- (13) Baraldi, P. G.; Fruttarolo, F.; Tabrizi, M. A.; Preti, D.; Romagnoli, R.; El-Kashef, H.; Moorman, A.; Varani, K.; Gessi, S.; Merighi, S.; Borea, P. A. Design, synthesis and biological

- evaluation of C⁹ and C² substituted pyrazolo[4,3-*e*]-1,2,4-triazolo[1,5-*c*]pyrimidines as new A_{2A} and A₃ adenosine receptor antagonists. *J. Med. Chem.* **2003**, *46*, 1229–1241.
- (14) Colotta, V.; Catarzi, D.; Varano, F.; Cecchi, L.; Filacchioni, G.; Martini, C.; Trincavelli, L.; Lucacchini, A. 1,2,4-Triazolo[4,3-*a*]quinoxalin-1-one: A Versatile Tool for the Synthesis of Potent and Selective Adenosine Receptor Antagonists. *J. Med. Chem.* **2000**, *43*, 1158–1164.
- (15) Lenzi, O.; Colotta, V.; Catarzi, D.; Varano, F.; Filacchioni, G.; Martini, C.; Trincavelli, L.; Ciampi, O.; Varani, K.; Marighetti, F.; Morizzo, E.; Moro, S. 4-Amido-2-aryl-1,2,4-triazolo[4,3-*a*]quinoxalin-1-ones as New Potent and Selective Human A₃ Adenosine Receptor Antagonists. Synthesis, Pharmacological Evaluation, and Ligand–Receptor Modeling Studies. *J. Med. Chem.* **2006**, *49*, 3916–3925.
- (16) Colotta, V.; Catarzi, D.; Varano, F.; Capelli, F.; Lenzi, O.; Filacchioni, G.; Martini, C.; Trincavelli, L.; Ciampi, O.; Pugliese, A. M.; Pedata, F.; Schiesaro, A.; Morizzo, E.; Moro, S. New 2-Arylpyrazolo[3,4-*c*]quinoline Derivatives as Potent and Selective Human A₃ Adenosine Receptor Antagonists. Synthesis, Pharmacological Evaluation, and Ligand–Receptor Modeling Studies. *J. Med. Chem.* **2007**, *50*, 4061–4074.
- (17) Colotta, V.; Lenzi, O.; Catarzi, D.; Varano, F.; Filacchioni, G.; Martini, C.; Trincavelli, L.; Ciampi, O.; Pugliese, A. M.; Traini, C.; Pedata, F.; Morizzo, E.; Moro, S. Pyrido[2,3-*e*]-1,2,4-triazolo[4,3-*a*]pyrazin-1-one as New Scaffold to Develop Potent and Selective Human A₃ Adenosine Receptor Antagonists. Synthesis, Pharmacological Evaluation and Ligand–Receptor Modeling Studies. *J. Med. Chem.* **2009**, *52*, 2407–2419.
- (18) Da Settimo, F.; Primofiore, G.; Taliani, S.; Marini, A. M.; La Motta, C.; Simorini, F.; Salerno, S.; Sergianni, V.; Tuccinardi, T.; Martinelli, A.; Cosimelli, B.; Greco, G.; Novellino, E.; Ciampi, O.; Trincavelli, M. L.; Martini, C. 5-Amino-2-phenyl[1,2,3]triazolo[1,2-*a*][1,2,4]benzotriazin-1-one: A Versatile Scaffold to Obtain Potent and Selective A₃ Adenosine Receptor Antagonists. *J. Med. Chem.* **2007**, *50*, 5676–5684.
- (19) Erve, J. C. L.; Vashishtha, S. C.; DeMaio, W.; Talaat, R. E. Metabolism of Prazosin in Rat, Dog, and Human Liver Microsomes and Cryopreserved Rat and Human Hepatocytes and Characterization of Metabolites by Liquid Chromatography/Tandem Mass Spectrometry. *Drug Metab. Dispos.* **2007**, *35*, 908–916.
- (20) Williams, D. P.; Antoine, D. J.; Butler, P. J.; Jones, R.; Randle, L.; Payne, A.; Howard, M.; Gardner, I.; Blagg, J.; Park, B. K. The Metabolism and Toxicity of Furosemide in the Wistar Rat and CD-1 Mouse: a Chemical and Biochemical Definition of the Toxicophore. *J. Pharmacol. Exp. Ther.* **2007**, *322*, 1208–1220.
- (21) Le Fur, J. M.; Labaune, J. P. Metabolic pathway by cleavage of a furan ring. *Xenobiotica* **1985**, *15*, 567–577.
- (22) Jaakola, V. P.; Griffith, M. T.; Hanson, M. A.; Cherezov, V.; Chien, E. Y. T.; Lane, J. R.; Ijzerman, A. P.; Stevens, R. C. The 2.6 Ångstrom Crystal Structure of a Human A_{2A} Adenosine Receptor Bound to an Antagonist. *Science* **2008**, *322*, 1211–1217.
- (23) Baraldi, P. G.; Bovero, A.; Fruttarolo, F.; Romagnoli, R.; Tabrizi, M. A.; Pretia, D.; Varani, K.; Borea, P. A.; Moorman, A. R. New Strategies for the Synthesis of A₃ Adenosine Receptor Antagonists. *Bioorg. Med. Chem.* **2003**, *11*, 4161–4169.
- (24) Klotz, K. N.; Hessling, J.; Hegler, J.; Owman, C.; Kull, B.; Fredholm, B. B.; Lohse, M. J. Comparative pharmacology of stably transfected receptors in CHO cells. *Naunyn-Schmiedeberg's Arch. Pharmacol.* **1998**, *357*, 1–9.
- (25) Klotz, K. N.; Cristalli, G.; Grifantini, M.; Vittori, S.; Lohse, M. J. Photoaffinity labeling of A₁ adenosine receptors. *J. Biol. Chem.* **1985**, *260*, 14659–14664.
- (26) De Lean, A.; Hancock, A. A.; Lefkowitz, R. J. Validation and statistical analysis of a computer modeling method for quantitative analysis of radioligand binding data for mixtures of pharmacological receptor subtypes. *Mol. Pharmacol.* **1982**, *21*, 5–16.
- (27) Cheng, Y. C.; Prusoff, H. R. Relationships between the inhibition constant (K_i) and the concentration of inhibitor which causes 50% inhibition (IC₅₀) of an enzymatic reaction. *Biochem. Pharmacol.* **1973**, *22*, 3099–3108.
- (28) Lenzi, O.; Colotta, V.; Catarzi, D.; Varano, F.; Poli, D.; Filacchioni, G.; Varani, K.; Vincenzi, F.; Borea, P. A.; Paoletta, S.; Morizzo, E.; Moro, S. 2-Phenylpyrazolo[4,3-*d*]pyrimidin-7-one as a New Scaffold to Obtain Potent and Selective Human A₃ Adenosine Receptor Antagonists: New Insights into the Receptor–Antagonist Recognition. *J. Med. Chem.* **2009**, *52*, 7640–7652.
- (29) Morizzo, E.; Federico, S.; Spalluto, G.; Moro, S. Human A₃ adenosine receptor as versatile G protein-coupled receptor example to validate the receptor homology modeling technology. *Curr. Pharm. Des.* **2009**, *15*, 4069–4084.
- (30) Baraldi, P. G.; Cacciari, B.; Moro, S.; Spalluto, G.; Pastorin, G.; Da Ros, T.; Klotz, K. N.; Varani, K.; Gessi, S.; Borea, P. A. Synthesis, Biological Activity, and Molecular Modeling Investigation of New Pyrazolo[4,3-*e*]-1,2,4-triazolo[1,5-*c*]pyrimidine Derivatives as Human A₃ Adenosine Receptor Antagonists. *J. Med. Chem.* **2002**, *45*, 770–780.
- (31) Baraldi, P. G.; Cacciari, B.; Spalluto, G.; de las Infantas y Villatoro, M. J. P.; Zocchi, C.; Dionisotti, S.; Ennio, O. Pyrazolo[4,3-*e*]-1,2,4-triazolo[1,5-*c*]pyrimidine Derivatives: Potent and Selective A_{2A} Adenosine Antagonists. *J. Med. Chem.* **1996**, *39*, 1164–1171.
- (32) Gao, Z.-G.; Chen, A.; Barak, D.; Kim, S.-K.; Muller, C. E.; Jacobson, K. A. Identification by site-directed mutagenesis of residues involved in ligand recognition and activation of the human A₃ adenosine receptor. *J. Biol. Chem.* **2002**, *277*, 19056–19063.
- (33) Kim, J.; Wess, J.; van Rhee, M.; Schoneberg, T.; Jacobson, K. A. Site-directed mutagenesis identifies residues involved in ligand recognition in the human A_{2A} adenosine receptor. *J. Biol. Chem.* **1995**, *270*, 13987–13997.
- (34) Kim, J.; Jiang, Q.; Glashofer, M.; Yehle, S.; Wess, J.; Jacobson, K. A. Glutamate residues in the second extracellular loop of the human A_{2A} adenosine receptor are required for ligand recognition. *Mol. Pharmacol.* **1996**, *49*, 683–691.
- (35) Moro, S.; Hoffmann, C.; Jacobson, K. A. Role of the extracellular loops of G protein-coupled receptors in ligand recognition: a molecular modeling study of the human P2Y₁ receptor. *Biochemistry* **1999**, *38*, 3498–3507.
- (36) Bradford, M. M. A rapid sensitive method for the quantification of microgram quantities of protein utilizing the principle of protein dye-binding. *Anal. Biochem.* **1976**, *72*, 248–254.
- (37) MOE (Molecular Operating Environment), version 2008.10; Chemical Computing Group Inc.: 1010 Sherbrooke Street West, Suite 910, Montreal, Quebec, Canada H3A 2R7; <http://www.chemcomp.com>.
- (38) Stewart, J. J. P. MOPAC 7; Fujitsu Limited: Tokyo, 1993.
- (39) GOLD suite, version 4.0.1; Cambridge Crystallographic Data Centre: 12 Union Road, Cambridge CB2 1EZ, UK; <http://www.ccdc.cam.ac.uk>
- (40) Ballesteros, J. A.; Weinstein, H. Integrated methods for the construction of three dimensional models and computational probing of structure–function relationships in G-protein coupled receptors. *Methods Neurosci.* **1995**, *25*, 366–428.
- (41) Labute, P. Protonate3D: assignment of ionization states and hydrogen coordinates to macromolecular structures. *Proteins* **2009**, *75*, 187–205.
- (42) Halgren, T. A.; Myrphy, R. B.; Friesner, R. A.; Beard, H. S.; Frye, L. L.; Pollard, W. T. Glide: a new approach for rapid, accurate docking and scoring 1 methods and assessment of docking accuracy. *J. Med. Chem.* **2004**, *47*, 1739–1749.
- (43) Korb, O.; Stütze, T.; Exner, T. E. Empirical Scoring Functions for advanced Protein–Ligand Docking with PLANTS. *J. Chem. Inf. Model.* **2009**, *49*, 84–96.